PHYSICAL REVIEW B VOLUME 32, NUMBER 9 1 NOVEMBER 1985

Theory of inhomogeneous quantum systems. IV. Variational calculations of metal surfaces

E. Krotscheck*
Department of Physics, Texas A&M University, College Station, Texas 77843-4242

W. Kohn and Guo-Xin Qian†
Department of Physics and Institute for Theoretical Physics, University of California, Santa Barbara, California 93106
(Received 13 May 1985)

We present results of variational calculations for the jellium model of metal surfaces. The ground-state wave function is represented by a product of local one- and two-body functions and a model Slater function. The correlation functions and the single-particle orbitals entering the Slater determinant are calculated by an unconstrained optimization procedure. Results for the surface energy and the work function are somewhat higher than previously published values.

I. INTRODUCTION

Physical quantum systems like atoms, molecules, solids, solid surfaces, or nuclei generally have density distributions $\rho_1(\mathbf{r})$, which are spatially strongly inhomogeneous. Whereas relatively small systems, like atoms, can be theoretically treated by traditional approximation methods like the Hartree-Fock equations, the Rayleigh-Ritz variational method, configuration space interaction, etc., these methods cannot be applied to systems consisting of an infinite (or very large) number of particles, like solids. For such systems, density-functional theory[1] (DFT) has proved to be a simple and very useful approach. Most calculations of the electronic structure of solids, solid surfaces, etc. in the last 10 to 20 years have used this method.

While density-functional theory is formally exact, for practical purposes approximations to the exchange-correlation functional $E_{\rm xc}[\rho_1(\mathbf{r})]$ must be made. The most common is the local-density approximation, which is based on the assumption that the density $\rho_1(\mathbf{r})$ varies slowly as a function of $\mathbf{r}$. Several useful corrections have been developed,[2] but the assumption of a relatively slow spatial variation of $\rho_1(\mathbf{r})$ underlies all of them. Although this assumption is not well satisfied in typical physical systems, results have been rather satisfactory.

In this paper we approach the problem of inhomogeneous systems using the (Fermi) hypernetted-chain (FHNC) equations. Whereas DFT, by construction, is "exact" for homogeneous systems, FHNC theory is not because it approximates correlation effects by a two-particle Jastrow correlation $u_2(|\mathbf{r}_i-\mathbf{r}_j|)$ and calculates the energy expectation value in an approximate manner. However, the errors are very small for the homogeneous electron gas.[3] In contrast to DFT, FHNC theory does *not* assume slow spatial variation of the one-body density $\rho_1(\mathbf{r})$. One may therefore expect that, when applied to large, strongly nonuniform systems, it will lead to results whose accuracy is comparable to the very high accuracy obtained for homogeneous systems. In the present paper we show that the solution of the FHNC equations, including the optimization of the correlation function $u_2(\mathbf{r}_1,\mathbf{r}_2)$, for inhomogeneous systems is, in fact, feasible. Although the computational effort is very much larger than in a DFT calculation, we found, for the case of metal surfaces, that all calculations reported in this paper could be carried out in about 250 h of VAX 780 time.

This paper reports on progress in the application of a variational theory developed earlier (Refs. 4, 5, and 6, hereafter called papers I, II, and III, respectively) for inhomogeneous Bose and Fermi systems. Our previous work dealt with the theoretical development for both Bose[4] and Fermi[6] systems, and numerical application of the theory to the structure[4] and the collective excitations[5] of the free surface and films of liquid ^{4}He. The variational approach to metal surfaces has been pioneered by Woo and collaborators,[7,8] who start from the same *ansatz* for the wave function. Our theory differs from the one by Woo in that it uses the more common Fermi hypernetted-chain method[9] for the summation of infinite classes of diagrams, and involves the optimization of the single-particle basis and the two-body correlations through Euler-Lagrange equations. It is one of the most appealing aspects of the hypernetted-chain theory that this optimization hardly complicates the calculations. This paper presents the first application of the Fermi hypernetted-chain theory for inhomogeneous systems to the case of the electron gas in a metal surface.

In the simplest model of a metal, one assumes that the ion lattice is static and may be represented by a distribution $\rho_+(\mathbf{r})$. The Hamiltonian of the system is then

$$H=-\sum_i \frac{\hbar^2}{2m}\nabla_i^2+\tfrac{1}{2}\int d^3r_1\int d^3r_2\,\rho_+(\mathbf{r}_1)\rho_+(\mathbf{r}_2)v_C(|\mathbf{r}_1-\mathbf{r}_2|)-\sum_i\int d^3r\,v_C(|\mathbf{r}_i-\mathbf{r}|)\rho_+(\mathbf{r})+\tfrac{1}{2}\sum_{\substack{i<j\\ i,j}} v_C(|\mathbf{r}_i-\mathbf{r}_j|)\,. \tag{1.1}$$

Here, $v_C(r)\equiv e^2/r$. The simplest jellium model of a metal surface assumes that the background charge $\rho_+(\mathbf{r})$ is a step function.

The variational method for an interacting many-particle system starts with an explicit *ansatz* for the ground-state wave functions, usually of the Feenberg form[10]

$$|\Psi_0\rangle=\exp\left[\frac{1}{2}\sum_i u_1(\mathbf{r}_i)+\frac{1}{2}\sum_{\substack{i<j\\ i,j}} u_2(\mathbf{r}_i,\mathbf{r}_j)+\cdots\right]|\Phi_0\rangle/\mathcal{N}\,, \tag{1.2}$$

($\mathcal{N}$ is the norm) which is made unique by requiring that each of the $u_i(\mathbf{r}_1,\mathbf{r}_2,\ldots,\mathbf{r}_i)$ $(i>1)$ satisfies the *cluster property.*[10] $|\Phi_0\rangle$ is the ground-state wave function of a suitably chosen model system which reflects the *statistics* and the *symmetries* of the physical system under consideration. In the Fermi system under consideration here, the "noninteracting" model state $|\Phi_0\rangle$ is the determinant of a set of single-particle orbitals $\phi_i(j)\equiv\phi_i(\mathbf{r}_j)\chi(i)$ $(i,j=1,2,\ldots,A)$, i.e.,

$$|\Phi_0\rangle=\det|\phi_i(\mathbf{r}_j)\chi(i)|\,. \tag{1.3}$$

The $\chi(i)$ are the spin eigenfunctions. The spatial single-particle orbitals $\phi_i(\mathbf{r}_j)$ are usually generated by a one-body equation

$$H_0[\phi_k]\phi_i(\mathbf{r}_j)=\epsilon_i\phi_i(\mathbf{r}_j)\,, \tag{1.4}$$

where, as in Hartree or Hartree-Fock theory, $H_0[\phi_k]$ is a functional of the single-particle orbitals. In a sense, the one-body factor $u_1(\mathbf{r})$ is redundant; we have shown in paper III that it can always be absorbed in the model state by a suitable unitary transformation of the single-particle basis. But it is very useful to retain this factor and use the additional flexibility to construct a cluster expansion which is as compact as possible. An intermediate consequence of this construction is, as we will see, that the "Hartree" density calculated from the single-particle basis $\phi_i(j)$ is as close as possible to the true one-body density.

The n-body functions $u_1(\mathbf{r})$, $u_2(\mathbf{r}_i,\mathbf{r}_j),\ldots$ are determined by minimization of the ground-state energy,

$$\frac{\delta\langle\Psi_0|H|\Psi_0\rangle}{\delta u_n(\mathbf{r}_1,\ldots,\mathbf{r}_n)}=0\quad(n=1,2,\ldots)\,. \tag{1.5}$$

We will be concerned here mostly with $n=2$; the special role of the one-body function $u_1(r)$ will be reviewed in some detail below. In addition, the energy expectation value can be minimized with respect to the single-particle orbitals $\phi_i(j)$, which leads to a generalized Hartree-Fock equation.

Our paper is organized as follows. The next section reviews the results of paper III to the extent that they are specific to inhomogeneous systems. Special attention is paid to the construction of an optimal single-particle basis $\{\phi_i(\mathbf{r}_j)\}$. We demonstrate the important role of the one-body function $u_1(\mathbf{r})$ which may be used to cancel certain classes of reducible diagrams and to produce, thereby, a very compact cluster expansion.

Section III discusses briefly the equations that must be solved for the determination of the optimal two-body correlations, and discusses the FHNC//0 approximation which we use to connect the pair correlation factor $u_2(\mathbf{r}_1,\mathbf{r}_2)$ to the observable one- and two-body densities. Section IV gives the working formulas used for the energy expectation value, and presents the essential steps in the derivation of the one-body Hamiltonian which determines the single-particle wave functions. Section V presents our results for the one-body densities, pair-distribution and correlation functions, energies, surface energies, and work functions for the jellium models of metal slabs. At this level, we discuss only briefly ion-lattice corrections since we feel that the jellium model, while not providing a completely realistic picture of a real metal, is the most cleanly defined problem. Section VI reviews our results and prospects for further investigations.

Appendix A presents the formulation of the FHNC//0 equations for the infinite systems, and gives results for the ground-state energies for the same materials as considered in our computations for metal films. Appendix B gives some details on the numerical solution of the Euler-Lagrange equation for the two-body correlations, and Appendix C discusses our approximate treatment of the nonlocal Fock term.

II. SINGLE-PARTICLE WAVE FUNCTIONS

The derivation of cluster expansions and partial summations for the energy expectation value of the Hamiltonian (1.1),

$$H_{00}=\langle\Psi_0|H|\Psi_0\rangle\,, \tag{2.1}$$

with respect to the wave function (1.2) is most conveniently performed using a graphical representation. In paper III, we generalized the diagrammatic methods[11,12] used in the FHNC theory of bulk quantum liquids to formulate the Euler Lagrange equations for the optimal two-body correlations $u_2(\mathbf{r}_i,\mathbf{r}_j)$, to determine the most convenient choice of the one-body function $u_1(\mathbf{r})$, and to derive a generalized Hartree-Fock equation for the single-particle orbitals. This section and the next one are devoted to a brief review of these formal developments.

In the absence of a one-body function $u_1(\mathbf{r})$, the only reference to the model Slater function is through the one-body density matrix

$$\rho_1^F(\mathbf{r},\mathbf{r}')\equiv\sum_k n(k)\phi_k^*(\mathbf{r})\phi_k(\mathbf{r}')\,. \tag{2.2}$$

We have abbreviated the single-particle orbitals $\phi_i(\mathbf{r})\chi(i)$ by their labels i; $n(k)$ (0,1) is the occupation number of the kth orbital. In the presence of a one-body function, one defines

$$h_1(\mathbf{r})=\exp[u_1(\mathbf{r})]-1 \tag{2.3}$$

and a generalized one-body density matrix

$$\rho_1^F(u_1\,|\,\mathbf{r},\mathbf{r}')\equiv[1+h_1(\mathbf{r})]^{1/2}\left\{\rho_1(\mathbf{r},\mathbf{r}')-\frac{1}{\nu}[\rho_1^F*h_1*\rho_1^F](\mathbf{r},\mathbf{r}')+\frac{1}{\nu^2}[\rho_1^F*h_1*\rho_1^F*h_1*\rho_1^F](\mathbf{r},\mathbf{r}')-\cdots\right\}[1+h_1(\mathbf{r}')]^{1/2}\,, \tag{2.4}$$

where ν is the degeneracy of the single-particle states. For the electrons under consideration here, $\nu=2$.

We have introduced here a shorthand notation for convolution products of two-point functions. For a pair of two-point functions $A(\mathbf{r}_1,\mathbf{r}_2)$ and $B(\mathbf{r}_1,\mathbf{r}_2)$ we define

$$[A*B](\mathbf{r}_1,\mathbf{r}_2)\equiv\int d^3r_3 A(\mathbf{r}_1,\mathbf{r}_3)B(\mathbf{r}_3,\mathbf{r}_2)\,. \tag{2.5}$$

Functions of one variable are interpreted as diagonal, i.e., $h_1(\mathbf{r})\equiv h_1(\mathbf{r})\delta(\mathbf{r}-\mathbf{r}')$. Note that, for $u_1(\mathbf{r})=0$, $\rho_1^F(0\,|\,\mathbf{r},\mathbf{r}')\equiv\rho_1^F(\mathbf{r},\mathbf{r}')$. It was shown in paper III that the construction $\rho_1^F(u_1\,|\,\mathbf{r},\mathbf{r}')$ has the spectral representation

$$\rho_1^F(u_1\,|\,\mathbf{r},\mathbf{r}')=\sum_i n(i)\psi_i^*(u_1\,|\,\mathbf{r})\psi_i(u_1\,|\,\mathbf{r}')\,, \tag{2.6}$$

where the $\psi_i(u_1\,|\,\mathbf{r})$ are a set of single-particle wave functions, i.e., $\rho_1^F(u_1\,|\,\mathbf{r},\mathbf{r}')$ is, in fact, for all $u_1(\mathbf{r})$ the density matrix derived from a Slater determinant of single-particle orbitals $\psi_i(u_1\,|\,\mathbf{r})$.

Cluster contributions to the "generating functional"

$$G[u_1,u_2]\equiv\ln\langle\Phi_0|\,\exp\left[\sum_i u_1(\mathbf{r}_i)+\sum_{i<j}u_2(\mathbf{r}_i,\mathbf{r}_j)\right]|\,\Phi_0\rangle\,, \tag{2.7}$$

the one- and two-body densities

$$\rho_1(\mathbf{r}_1)=A\frac{\int d^3r_2\int d^3r_3\cdots\int d^3r_A\,|\,\Psi_0(\mathbf{r}_1,\mathbf{r}_2,\ldots,\mathbf{r}_A)\,|^2}{\int d^3r_1\int d^3r_2\cdots\int d^3r_A\,|\,\Psi_0(\mathbf{r}_1,\mathbf{r}_2,\ldots,\mathbf{r}_A)\,|^2}\,, \tag{2.8}$$

and

$$\rho_2(\mathbf{r}_1,\mathbf{r}_2)=A(A-1)\frac{\int d^3r_3\int d^3r_4\cdots\int d^3r_A\,|\,\Psi_0(\mathbf{r}_1,\mathbf{r}_2,\ldots,\mathbf{r}_A)\,|^2}{\int d^3r_1\int d^3r_2\cdots\int d^3r_A\,|\,\Psi_0(\mathbf{r}_1,\mathbf{r}_2,\ldots,\mathbf{r}_A)\,|^2}\,, \tag{2.9}$$

and the two-body distribution function

$$g(\mathbf{r}_1,\mathbf{r}_2)=\frac{\rho_2(\mathbf{r}_1,\mathbf{r}_2)}{\rho_1(\mathbf{r}_1)\rho_1(\mathbf{r}_2)} \tag{2.10}$$

are most conveniently represented as diagrams using the following graphical elements.

(i) Small open circles ("external" or "reference" points) represent the coordinates of particles. Solid circles ("internal" or "field" points) involve an integration over the coordinate space of that particle and a spin sum. (We deviate here from the usual convention which includes a density factor.)

(ii) Dashed lines ("correlation lines") between two circles i and j represent dynamical correlations

$$h_2(\mathbf{r}_i,\mathbf{r}_j)=\exp[u_2(\mathbf{r}_i,\mathbf{r}_j)]-1\,.$$

(iii) Solid, oriented lines from point i to point j represent dressed one-body density matrices ("exchange lines") $\rho_1^F(u_1\,|\,\mathbf{r}_i,\mathbf{r}_j)$.

The expansion of G in terms of correlation functions and exchange functions (one-body density matrices) is represented by the set of all topologically distinct connected diagrams without external points constructed according to the following rules:

(iv) Each n-body diagram (i.e., a diagram containing n points) has a counting factor $1/n!$.

(v) Each point is attached to at least one correlation line $h_2(\mathbf{r}_i,\mathbf{r}_j)$. Two different points may be connected by at most one correlation factor.

(vi) Each point is attached to exactly one incoming and one outgoing exchange line.

(vii) Exchange lines occur always in closed polygons and carry a factor $(-\nu)^{1-n}$, where n is the number of points connected by the exchange loop.

These rules are closely related to the corresponding rules for homogeneous Fermi systems.[11,12] The essential new feature is that the expansion contains reducible diagrams. (A diagram is called *reducible,* if, when cut at one point, it divides into two separate subdiagrams, one of which is not connected to any of the external points.) Otherwise, the same topological rules apply. In the case of the homogeneous system, the reducible diagrams cancel due to momentum conservation.

Figure 1 shows the diagrammatic representation of some of the simplest contributions to the generating functional G. Translating the graphical language into an algebraic form, the first diagram shown in Fig. 1 is

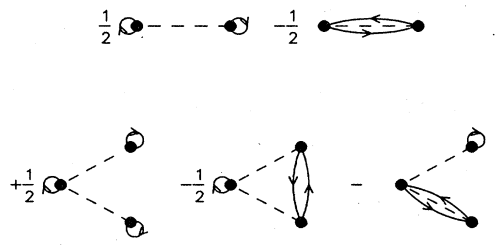

FIG. 1. Graphical representation of the first few terms of the cluster expansion of the generating functional G. Note that the directed line represents the function $\rho_1^F(u_1\,|\,\mathbf{r}_i,\mathbf{r}_j)$.

$$\Delta G_2^{(1)} = \int d^3r_1 d^3r_2 \rho_1^F(u_1 \mid \mathbf{r}_1,\mathbf{r}_1) \times \{\exp[u_2(\mathbf{r}_1,\mathbf{r}_2)]-1\}\rho_1^F(u_1 \mid \mathbf{r}_2,\mathbf{r}_2) , \tag{2.11}$$

whereas the second diagrams is

$$\Delta G_2^{(2)} = -\frac{1}{\nu}\int d^3r_1 d^3r_2 \rho_1^F(u_1 \mid \mathbf{r}_1,\mathbf{r}_2) \times \{\exp[u_2(\mathbf{r}_1,\mathbf{r}_2)]-1\}\rho_1^F(u_1 \mid \mathbf{r}_2,\mathbf{r}_1) . \tag{2.12}$$

From the generating functional G, one can conveniently derive expressions for the one- and two-body densities by functional variation with respect to the one-body function $u_1(\mathbf{r})$:

$$\frac{\delta G}{\delta u_1(\mathbf{r})} = \rho_1(\mathbf{r}) \tag{2.13}$$

and

$$\frac{\delta^2 G}{\delta u_1(\mathbf{r}_1)\delta u_1(\mathbf{r}_2)} = \rho_2(\mathbf{r}_1,\mathbf{r}_2) - \rho_1(\mathbf{r}_1)\rho_1(\mathbf{r}_2) . \tag{2.14}$$

We have to keep the dependence of $\rho_1^F(u_1 \mid \mathbf{r},\mathbf{r}')$ on $u_1(\mathbf{r})$ in mind when we calculate distribution functions by the functional variations (2.13) and (2.14); i.e., we must observe [cf. Eq. (2.4)] that

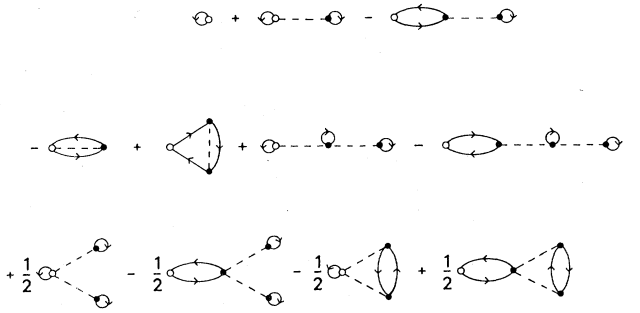

FIG. 2. Graphical representation of the first few terms of the cluster expansion of the one-body density.

$$\frac{\delta\rho_1^F(u_1 \mid \mathbf{r}_1,\mathbf{r}_2)}{\delta u_1(\mathbf{r})} = \tfrac{1}{2}\rho_1^F(u_1 \mid \mathbf{r}_1,\mathbf{r}_2)[\delta(\mathbf{r}_1-\mathbf{r})+\delta(\mathbf{r}-\mathbf{r}_2)] - \frac{1}{\nu}\rho_1^F(u_1 \mid \mathbf{r}_1,\mathbf{r})\rho_1^F(u_1 \mid \mathbf{r},\mathbf{r}_2) . \tag{2.15}$$

Using the construction (2.13)–(2.15), one finds that (a) the one-body density is represented by the sum of all diagrams having one "external" point, and (b) the two-body density is represented by the sum of all diagrams having two "external" points. The diagrammatic representation of the first few diagrams contributing to the one-body density is shown in Fig. 2. The first three terms in the expansion have the algebraic form

$$(\Delta\rho_1)_0^{(1)}(\mathbf{r}_1) = \rho_1^F(u_1 \mid \mathbf{r}_1,\mathbf{r}_1) , \tag{2.16}$$

$$(\Delta\rho_1)_1^{(1)}(\mathbf{r}_1) = \rho_1^F(u_1 \mid \mathbf{r}_1,\mathbf{r}_1)\int d^3r_2\{\exp[u_2(\mathbf{r}_1,\mathbf{r}_2)]-1\}\rho_1^F(u_1 \mid \mathbf{r}_2,\mathbf{r}_2) , \tag{2.17}$$

$$(\Delta\rho_1)_1^{(2)}(\mathbf{r}_1) = \int d^3r_2 d^3r_3 \rho_1^F(u_1 \mid \mathbf{r}_1,\mathbf{r}_2)\rho_1^F(u_1 \mid \mathbf{r}_2,\mathbf{r}_1)\{\exp[u_2(\mathbf{r}_2,\mathbf{r}_3)]-1\}\rho_1^F(u_1 \mid \mathbf{r}_3,\mathbf{r}_3) . \tag{2.18}$$

Attention is now directed to the special set of corrections to the one-body density beyond the Hartree-Fock approximation (first diagram of Fig. 2) that contains one factor $\rho_1^F(u_1 \mid \mathbf{r},\mathbf{r})$. Examples of such structures are the second, sixth, eighth, and the tenth diagram shown in Fig. 2. We write the sum of all these diagrams as

$$\rho_1^F(u_1 \mid \mathbf{r},\mathbf{r})\{\exp[\gamma(\mathbf{r})]-1\} .$$

The structures, such as shown in Fig. 3, contributing to the factor $\{\exp[\gamma(\mathbf{r})]-1\}$, also occur in other diagrams, e.g., diagrams 3, 7, 9, and 11 of Fig. 2. These diagrams are called *"d-reducible."* Figure 4(a) shows a d-reducible diagram, Fig. 4(b) a reducible (but not d-reducible) diagram, both contributing to the two-body density. The occurrence of d-reducible diagrams along any exchange path suggests the introduction of a dressed exchange function $\rho_1^F(u_1+\gamma \mid \mathbf{r},\mathbf{r}')$, which sums all these diagrams. Examples of diagrams included in the dressed exchange function are shown in Fig. 5. The dressing procedure is analogous to the one performed in the derivation of $\rho_1^F(u_1 \mid \mathbf{r},\mathbf{r}')$ in Eq. (2.4). The algebraic definition of $\rho_1^F(u_1+\gamma \mid \mathbf{r},\mathbf{r}')$ is

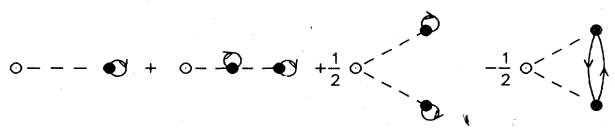

FIG. 3. Graphical representation of the first few contributions to $\exp[\gamma(\mathbf{r})]-1$.

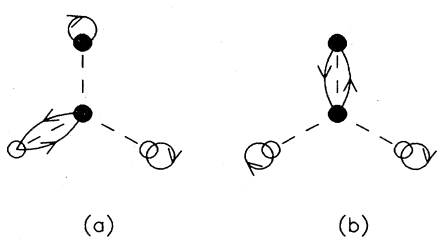

FIG. 4. Two contributions to the pair correlation function $g(\mathbf{r}_1,\mathbf{r}_2)$. Diagram (a) is "$d$-reducible"; diagram (b) is not.

$$\rho_1^F(u_1+\gamma\,|\,\mathbf{r},\mathbf{r}')=[1+h_\gamma(\mathbf{r})]^{1/2}\left\{\rho_1^F(u=0\,|\,\mathbf{r},\mathbf{r}')-\frac{1}{\nu}[\rho_1^F(u=0)*h_\gamma*\rho_1^F(u=0)](\mathbf{r},\mathbf{r}')+\cdots\right\}[1+h_\gamma(\mathbf{r}')]^{1/2}\,, \quad (2.19)$$

with

$$h_\gamma(\mathbf{r})\equiv\exp[u_1(\mathbf{r})+\gamma(\mathbf{r})]-1\equiv\exp[u_\gamma(\mathbf{r})]-1\,. \quad (2.20)$$

One may now reformulate the cluster-expansions for the generating functional and the one- and two-body densities in terms of this new, generalized density matrix. The modified diagrammatic rules are the following:

(iii) Solid, oriented lines from point i to point j represent one-body density matrices ("exchange lines") $\rho_1^F(u_1+\gamma\,|\,\mathbf{r}_i,\mathbf{r}_j)$.

(vii) No d-reducible diagrams occur.

For given functions $u_1(\mathbf{r})$, $u_2(\mathbf{r}_i,\mathbf{r}_j)$, the dressed exchange line must still be calculated, but the task is considerably simplified by the optimal choice of the single-particle basis: We have shown in paper III that the optimal single-particle basis is generated by the generalized Hartree-Fock equation

$$\left[\frac{\hbar^2}{2m}\nabla^2+U_{\rm ext}(\mathbf{r})\right]\phi_i(\mathbf{r})+\int d^3\mathbf{r}_1\frac{\delta[E_2+T_{\rm JF}]}{\delta\rho_1^F(u_1=0\,|\,\mathbf{r},\mathbf{r}_1)}\phi_i(\mathbf{r}_1)=\epsilon_i\phi_i(\mathbf{r})\,, \quad (2.21)$$

where

$$E_2=\tfrac{1}{2}\int d^3r_1\int d^3r_2\,\rho_2(\mathbf{r}_1,\mathbf{r}_2)[v_C(\,|\,\mathbf{r}_1-\mathbf{r}_2\,|\,)+t_{\rm JF}(\mathbf{r}_1,\mathbf{r}_2)] \quad (2.22)$$

with the Jackson-Feenberg kinetic-energy correction

$$t_{\rm JF}(\mathbf{r}_1,\mathbf{r}_2)=-\frac{\hbar^2}{8m}[D(1)+D(2)]u_2(\mathbf{r}_1,\mathbf{r}_2)\,, \quad (2.23)$$

$$D(i)\equiv\frac{1}{\rho_1(\mathbf{r}_i)}\nabla_{\mathbf{r}_i}\rho_1(\mathbf{r}_i)\cdot\nabla_{\mathbf{r}_i}\,, \quad (2.24)$$

and

$$T_{\rm JF}=\frac{\hbar^2}{8m}\int d^3r\,\nabla_F^2\rho_1(\mathbf{r})\,. \quad (2.25)$$

In Eq. (2.25), the operator ∇_F differentiates in a graphical representation of the one-body density *only the exchange functions* attached to point $\mathbf{r}$. For example, the second diagram shown in Fig. 2 contributes a term

$$(\Delta T_{\rm JF})_2^{(1)}=-\frac{\hbar^2}{8m\nu}\int d^3r_1\int d^3r_2\rho_1^F(\mathbf{r}_2,\mathbf{r}_2)\times\{\exp[u_2(\mathbf{r}_1,\mathbf{r}_2)]-1\}\times\nabla_1^2\rho_1^F(\mathbf{r}_1,\mathbf{r}_1)\,. \quad (2.26)$$

This choice of the single-particle states leads to optimal one- and two-body functions, which satisfy the relation

$$u_1^{\rm opt}(\mathbf{r})+\gamma[u_1^{\rm opt},u_2^{\rm opt}](\mathbf{r})=0\,. \quad (2.27)$$

The determination of the single-particle states through Eq. (2.21) not only gives the lowest energy that can be obtained in the space of all correlated wave functions of the form (1.2), it also leads to the most compact cluster expansions in the sense that all d-reducible diagrams vanish. We assume from now on that we have chosen this basis, and omit all further reference to $u_1(\mathbf{r})$ and $\gamma(\mathbf{r})$, i.e., we write

$$\rho_1^F(u_\gamma^{\rm opt}=0\,|\,\mathbf{r}_1,\mathbf{r}_2)\equiv\rho_1^F(\mathbf{r}_1,\mathbf{r}_2)\,.$$

The one-body density in this basis is still not identical with the Hartree-Fock density $\rho_1^F(\mathbf{r},\mathbf{r})=\rho_1^F(u_\gamma=0\,|\,\mathbf{r},\mathbf{r})$, but many diagrams have been eliminated, which we would otherwise need to calculate. The elimination of these diagrams is, for *optimized* pair correlation functions, not only a matter of convenience: The sum of all d-reducible diagrams diverges for the long-ranged optimal correlation functions. The correct way to regularize this divergence is[8] to *first* take the zero-momentum limit, and then go to an infinite box size. The optimal choice of the single-particle states makes such a procedure unnecessary, but it will be needed if the optimal correlations calculated here are to be used in a more accurate Monte Carlo evaluation of the energy.

The remaining diagrams contributing to the one-body density (the same sets appear also as reducible diagrams contributing to the pair-distribution function) are of a quite different nature and must be kept together[6] with correction terms to the particle-hole propagators.

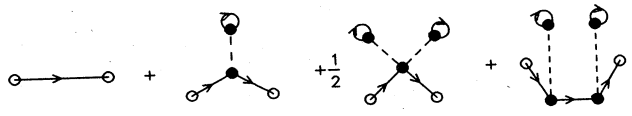

FIG. 5. Examples of the first diagrams summed in $\rho_1^F(u_1+\gamma\,|\,\mathbf{r}_i,\mathbf{r}_j)$. Note that the directed line represents the function $\rho_1^F(u_1\,|\,\mathbf{r}_i,\mathbf{r}_j)$.

III. TWO-BODY CORRELATIONS

The next step in the development of the theory is the calculation of distribution functions and the optimization of the two-body correlations. We have restricted ourselves in paper III to the simplest version of the FHNC theory of Ref. 9 (called FHNC//0), which sums ring and ladder diagrams, but omits corrections to the particle-hole propagators. The approximation works reasonably well[9] for liquid ^{3}He. Appendix A describes the implementation of the method for the bulk electron gas, we see there that the approximation is also quite satisfactory.

The FHNC//0 equations derived in paper III give a relation between the pair correlation function $u_2(\mathbf{r}_1,\mathbf{r}_2)$, the

static form factor of the model system

$$S_F(\mathbf{r}_1,\mathbf{r}_2)=\delta(\mathbf{r}_1-\mathbf{r}_2)-\frac{1}{\nu}\frac{|\rho_1^F(\mathbf{r}_1,\mathbf{r}_2)|^2}{[\rho_1^F(\mathbf{r}_1,\mathbf{r}_1)\rho_1^F(\mathbf{r}_2,\mathbf{r}_2)]^{1/2}}\ , \tag{3.1}$$

and the sets of "non-nodal" and "nodal" dd diagrams $X_{dd}(\mathbf{r}_1,\mathbf{r}_2)$ and $N_{dd}(\mathbf{r}_1,\mathbf{r}_2)$, respectively:

$$X_{dd}(\mathbf{r}_1,\mathbf{r}_2)=\exp[u_2(\mathbf{r}_1,\mathbf{r}_2)+N_{dd}(\mathbf{r}_1,\mathbf{r}_2)]-1-N_{dd}(\mathbf{r}_1,\mathbf{r}_2)\ , \tag{3.2}$$

$$\tilde{N}_{dd}(\mathbf{r}_1,\mathbf{r}_2)=[\tilde{X}_{dd}*S_F*\tilde{\Gamma}_{dd}](\mathbf{r}_1,\mathbf{r}_2)\ . \tag{3.3}$$

Here we have introduced for any two-point function $A(\mathbf{r}_1,\mathbf{r}_2)$ the abbreviation

$$\tilde{A}(\mathbf{r}_1,\mathbf{r}_2)\equiv[\rho_1(\mathbf{r}_1)]^{1/2}A(\mathbf{r}_1,\mathbf{r}_2)[\rho_1(\mathbf{r}_2)]^{1/2}\ , \tag{3.4}$$

and

$$\Gamma_{dd}(\mathbf{r}_1,\mathbf{r}_2)\equiv X_{dd}(\mathbf{r}_1,\mathbf{r}_2)+N_{dd}(\mathbf{r}_1,\mathbf{r}_2)\ . \tag{3.5}$$

In the same approximation, the static form factor of the interacting system is

$$S(\mathbf{r}_1,\mathbf{r}_2)=S_F(\mathbf{r}_1,\mathbf{r}_2)+[S_F*\tilde{\Gamma}_{dd}*S_F](\mathbf{r}_1,\mathbf{r}_2)\ . \tag{3.6}$$

The equations reduce to the Bose HNC equations for $S_F(\mathbf{r}_1,\mathbf{r}_2)=\delta(\mathbf{r}_1-\mathbf{r}_2)$. Using the FHNC//0 approximation (3.1)–(3.6), we have derived in paper III the Euler-Lagrange equation for the two-body quantities. Our formulation of the equation is the generalization of the corresponding equation for Bose systems derived in paper I: After some lengthy algebra[6] one arrives at the following final form of the Fermion Euler-Lagrange equation:

$$-[S_F^{-1}*H_1*\tilde{X}_{dd}+\tilde{X}_{dd}*H_1*S_F^{-1}-\tilde{X}_{dd}*H_1*\tilde{X}_{dd}](\mathbf{r}_1,\mathbf{r}_2)=2\tilde{V}_{\text{p-h}}(\mathbf{r}_1,\mathbf{r}_2)\ . \tag{3.7}$$

S_F^{-1} in Eq. (3.7) is the inverse of S_F in the sense of the convolution product (2.5), and

$$H_1\equiv-\frac{\hbar^2}{2m}\frac{1}{[\rho_1(\mathbf{r})]^{1/2}}\nabla\rho_1(\mathbf{r})\cdot\nabla\frac{1}{[\rho_1(\mathbf{r})]^{1/2}}\ . \tag{3.8}$$

The particle-hole interaction $V_{\text{p-h}}(\mathbf{r}_1,\mathbf{r}_2)$ can be expressed in terms of the bare two-body interaction $v_C(\mathbf{r}_1-\mathbf{r}_2)$ and the compound-diagrammatic quantities $X_{dd}(\mathbf{r}_1,\mathbf{r}_2)$, $N_{dd}(\mathbf{r}_1,\mathbf{r}_2)$, and $\Gamma_{dd}(\mathbf{r}_1,\mathbf{r}_2)$ introduced above:

$$\tilde{V}_{\text{p-h}}(\mathbf{r}_1,\mathbf{r}_2)=[\rho_1(\mathbf{r}_1)\rho_1(\mathbf{r}_2)]^{1/2}\left[[1+\Gamma_{dd}(\mathbf{r}_1,\mathbf{r}_2)]v_C(|\mathbf{r}_1-\mathbf{r}_2|)+\frac{\hbar^2}{2m}\{|\nabla_{\mathbf{r}_1}[1+\Gamma_{dd}(\mathbf{r}_1,\mathbf{r}_2)]^{1/2}|^2+|\nabla_{\mathbf{r}_2}[1+\Gamma_{dd}(\mathbf{r}_1,\mathbf{r}_2)]^{1/2}|^2\}\right]$$
$$-\tfrac{1}{2}\Gamma_{dd}(\mathbf{r}_1,\mathbf{r}_2)[\tilde{N}_{dd}*H_1*S_F^{-1}+S_F^{-1}*H_1*\tilde{N}_{dd}+\tilde{X}_{dd}*H_1*\tilde{X}_{dd}](\mathbf{r}_1,\mathbf{r}_2)\ . \tag{3.9}$$

Equations (3.7) and (3.9) form, together with the chain equation (3.3), a closed set of equations for the determination of the required two-body quantities from the bare two-body potential $v_C(|\mathbf{r}_1-\mathbf{r}_2|)$ and a given static form factor $S_F(\mathbf{r}_1,\mathbf{r}_2)$ for the model system. These may be solved numerically by a straightforward iteration; we describe the procedure in detail in Sec. V. We will refer to Eq. (3.7) as to the "paired-phonon-analysis" (PPA) equation since it is the generalization of the Bose paired-phonon-analysis equation originally derived by Campbell and Feenberg[13] for homogeneous Bose systems and extended by us to inhomogeneous Bose[4] and Fermi[6] systems.

IV. ENERGY CALCULATION AND ONE-BODY POTENTIALS

We present in this section the manipulations that are necessary to represent the ground-state energy and the Hartree-Fock potentials needed in Eq. (2.21) in a form that is convenient for further applications. The total energy in the FHNC approximation used in this paper has the form

$$E=T_F+E_{\text{es}}+E_x+E_c\ , \tag{4.1}$$

where

$$T_F=-\frac{\hbar^2}{2m}\sum_i\langle\Phi_0|\nabla_i^2|\Phi_0\rangle \tag{4.2}$$

is the kinetic energy,

$$E_{\text{es}}=\int d^3r_1\int d^3r_2[\rho_1(\mathbf{r}_1)-\rho_+(\mathbf{r}_1)]\times[\rho_1(\mathbf{r}_2)-\rho_+(\mathbf{r}_2)]v_C(|\mathbf{r}_1-\mathbf{r}_2|) \tag{4.3}$$

is the kinetic energy,

$$E_x=\tfrac{1}{2}\int d^3r_1\int d^3r_2[\rho_1(\mathbf{r}_1)\rho_1(\mathbf{r}_2)]^{1/2}\times[S_F(\mathbf{r}_1,\mathbf{r}_2)-\delta(\mathbf{r}_1-\mathbf{r}_2)]v_C(|\mathbf{r}_1-\mathbf{r}_2|) \tag{4.4}$$

is the exchange energy, all calculated in the optimized single-particle basis $\{\phi_i\}$, and

$$E_c=\int d^3r_1\int d^3r_2\{[\rho_2(\mathbf{r}_1,\mathbf{r}_2)-\rho_2^F(\mathbf{r}_1,\mathbf{r}_2)]v_C(|\mathbf{r}_1-\mathbf{r}_2|)+[\rho_2(\mathbf{r}_1,\mathbf{r}_2)-\rho_1(\mathbf{r}_1)\rho_1(\mathbf{r}_2)]t_{\text{JF}}(\mathbf{r}_1,\mathbf{r}_2)\}+T_{\text{JF}} \tag{4.5}$$

is the correlation energy [cf. Eq. (2.23) for the definition of t_{JF}]. $\rho_2^F(\mathbf{r}_1,\mathbf{r}_2)$ is the two-body density of the model system

$$\rho_2^F(\mathbf{r}_1,\mathbf{r}_2)=\rho_1^F(\mathbf{r}_1)\rho_1^F(\mathbf{r}_2)-\frac{1}{\nu}|\rho_1^F(\mathbf{r}_1,\mathbf{r}_2)|^2\ . \tag{4.6}$$

In the FHNC//0 approximation used here, the term T_{JF} has the simple form[6]

$$T_{\rm JF}=\frac{\hbar^2}{16m}\int d^3r_1 d^3r_2[\rho_2^F(\mathbf{r}_1,\mathbf{r}_2)-\rho_1(\mathbf{r}_1)\rho_1(\mathbf{r}_2)][D(1)+D(2)]\Gamma_{dd}(\mathbf{r}_1,\mathbf{r}_2)\ . \tag{4.7}$$

To isolate an "RPA energy," we write in $t_{\rm JF}$, Eq. (2.23),

$$u_2(\mathbf{r}_1,\mathbf{r}_2)=\ln[1+\Gamma_{dd}(\mathbf{r}_1,\mathbf{r}_2)]-\Gamma_{dd}(\mathbf{r}_1,\mathbf{r}_2)+X_{dd}(\mathbf{r}_1,\mathbf{r}_2)\ . \tag{4.8}$$

At the same time we add and subtract the particle-hole interaction and represent the correlation energy as

$$E_c=\Delta E_{\rm pot}+\Delta T_{\rm JF}+E_{\rm RPA} \tag{4.9}$$

with

$$\Delta E_{\rm pot}=\tfrac{1}{2}\int d^3r_1\int d^3r_2[\rho_2(\mathbf{r}_1,\mathbf{r}_2)-\rho_2^F(\mathbf{r}_1,\mathbf{r}_2)][v_C(|\mathbf{r}_1-\mathbf{r}_2|)-V_{\text{p-h}}(\mathbf{r}_1,\mathbf{r}_2)]\ , \tag{4.10}$$

$$\Delta T_{\rm JF}=-\tfrac{1}{2}\int d^3r_1\int d^3r_2[\rho_2(\mathbf{r}_1,\mathbf{r}_2)-\rho_1(\mathbf{r}_1)\rho_1(\mathbf{r}_2)]\frac{\hbar^2}{8m}[D(1)+D(2)]\{\ln[1+\Gamma_{dd}(\mathbf{r}_1,\mathbf{r}_2)]-\Gamma_{dd}(\mathbf{r}_1,\mathbf{r}_2)\}\ , \tag{4.11}$$

$$E_{\rm RPA}=\tfrac{1}{2}\int d^3r_1\int d^3r_2\left[[\rho_2(\mathbf{r}_1,\mathbf{r}_2)-\rho_2^F(\mathbf{r}_1,\mathbf{r}_2)]V_{\text{p-h}}(\mathbf{r}_1,\mathbf{r}_2)-[\rho_2(\mathbf{r}_1,\mathbf{r}_2)-\rho_1(\mathbf{r}_1)\rho_1(\mathbf{r}_2)]\frac{\hbar^2}{8m}[D(1)+D(2)]X_{dd}(\mathbf{r}_1,\mathbf{r}_2)\right.$$
$$\left.+[\rho_2^F(\mathbf{r}_1,\mathbf{r}_2)-\rho_1(\mathbf{r}_1)\rho_1(\mathbf{r}_2)]\frac{\hbar^2}{8m}[D(1)+D(2)]\Gamma_{dd}(\mathbf{r}_1,\mathbf{r}_2)\right]\ . \tag{4.12}$$

The last term (4.12) allows for a number of significant simplifications in which the Euler-Lagrange (PPA) equation (3.7) is used to eliminate $V_{\text{p-h}}(\mathbf{r}_1,\mathbf{r}_2)$. After a few elementary manipulations we arrive at the more convenient and compact form

$$E_{\rm RPA}=-\tfrac{1}{4}\int d^3r[S_F*\tilde{X}_{dd}*H_1*\tilde{X}_{dd}](\mathbf{r},\mathbf{r})\ . \tag{4.13}$$

In the high-density limit we can identify the particle-hole interaction, $V_{\text{p-h}}(\mathbf{r}_i,\mathbf{r}_j)$ with the bare Coulomb interaction, $v_C(|\mathbf{r}_i-\mathbf{r}_j|)$, so that by Eq. (4.10), $\Delta E_{\rm pot}=0$. Furthermore, we can neglect $|\Gamma_{dd}(\mathbf{r}_1,\mathbf{r}_2)|^2$ in comparison with $|\Gamma_{dd}(\mathbf{r}_1,\mathbf{r}_2)|$, so that, by Eq. (4.11), $\Delta T_{\rm JF}=0$. Thus, the correlation energy E_c, Eq. (4.9) is entirely given by $E_{\rm RPA}$. Equation (4.12) is the generalization of a similar expression given in Ref. 14 for the homogeneous electron gas.

Some care must be exercised in the choice of approximations for the distinct contributions to the correlation energy. A fully consistent implementation of the optimized FHNC equation requires summation or at least adequate estimates of three- and four-point functions, and involves a coupled system of eight integral equations. Here we do not attempt such an effort. As a consequence one must either live with slight inconsistencies between coordinate-space and momentum-space representations of the same quantity, or one must sacrifice exact properties either in coordinate or in momentum space. The issue has been discussed in detail in Ref. 14. The two energy contributions $E_{\rm RPA}$ and $\Delta T_{\rm JF}$ are typical examples: $E_{\rm RPA}$ sums the long-ranged quantities; it is therefore important to use an approximation that is exact in momentum space in the long-wavelength limit. This is clearly

$$\rho_2(\mathbf{r}_1,\mathbf{r}_2)\approx[\rho_1(\mathbf{r}_1)]^{1/2}[S_F*\tilde{\Gamma}_{dd}*S_F](\mathbf{r}_1,\mathbf{r}_2)[\rho_1(\mathbf{r}_2)]^{1/2}$$
$$+\rho_2^F(\mathbf{r}_1,\mathbf{r}_2)\ .$$

On the other hand, the term

$$\ln[1+\Gamma_{dd}(\mathbf{r}_1,\mathbf{r}_2)]-\Gamma_{dd}(\mathbf{r}_1,\mathbf{r}_2)$$

is short ranged; in fact, it is very large for small distances $|\mathbf{r}_1-\mathbf{r}_2|$. Therefore, it is important to keep the common factor $1+\Gamma_{dd}(\mathbf{r}_1,\mathbf{r}_2)$ which occurs in the FHNC expression for the two-body density, in order to screen the short-range structure. The simplest way to do this is to keep just the term $1+\Gamma_{dd}(\mathbf{r}_1,\mathbf{r}_2)$ in the pair-distribution function occurring in $\Delta T_{\rm JF}$. This leads to the compact representation

$$\Delta T_{\rm JF}=-\frac{\hbar^2}{4m}\int d^3r_1\int d^3r_2\,\rho_1(\mathbf{r}_1)\rho_1(\mathbf{r}_2)\Gamma_{dd}(\mathbf{r}_1,\mathbf{r}_2)$$
$$\times\{|\nabla_1[1+\Gamma_{dd}(\mathbf{r}_1,\mathbf{r}_2)]^{1/2}|^2$$
$$+|\nabla_2[1+\Gamma_{dd}(\mathbf{r}_1,\mathbf{r}_2)]^{1/2}|^2\}\ . \tag{4.14}$$

The approximation obtained in this way for the ground-state energy is not quite as good as can be obtained in a more elaborate[14] FHNC/C calculation, but it is reasonable and probably sufficient for our further purposes. Appendix A gives the bulk limit of the Euler-Lagrange equations and the approximation for the energy derived above, and a comparison of energies for the bulk electron liquid between Green's-function Monte Carlo (GFMC), RPA, the best FHNC calculation, and the present approximation.

To conclude the formal parts of this work, we now derive the expressions for the Hartree and Fock terms needed in the one-body equation (2.21). It is most convenient to use diagrammatic arguments. As in the derivation of the two-body equations (3.7) and (3.9), we start from the energy expectation value [(4.1)–(4.7)]. The functional derivative of the ground-state density with respect to $\rho_1^F(\mathbf{r}_1,\mathbf{r}_2)$ consists of two parts, (a) the Hartree term, which combines all contributions in which the variational derivative (2.21) is carried out with respect to a degenerate exchange loop $\rho_1^F(\mathbf{r},\mathbf{r})$, and (b) the Fock term con-

taining the variational derivatives of diagrams having nondegenerate exchange lines $\rho_1^F(\mathbf{r}_1,\mathbf{r}_2)$. The algebraic manipulations are somewhat tedious and will be sketched here only briefly. Consistent with the present level of FHNC approximation, we identify $\rho_1(\mathbf{r})=\rho_1^F(\mathbf{r},\mathbf{r})$.

The variation of the Coulomb energy with respect to the one-body density gives rise to the familiar Hartree term of the Hartree-Fock approximation:

$$V_H^{(0)}\equiv\frac{\delta E_{\rm es}}{\delta\rho(\mathbf{r})}=\int d^3r_1[\rho_1(\mathbf{r}_1)-\rho_+(\mathbf{r}_1)]v_C(|\mathbf{r}-\mathbf{r}_1|)\ . \tag{4.15}$$

The variational derivative of the correlation energy E_c gives three structurally different contributions, arising from the following: (a) The derivative of the expression (4.5) with respect to the one-body density appearing as a factor of $v_C(|\mathbf{r}_1-\mathbf{r}_2|)$. Note that this term contains only diagrammatic contributions to the two-body density, where a degenerate exchange line is attached to the external point. Consequently, there is no contribution from $T_{\rm JF}$ to this term, which can be written in the form

$$V_H^{(1')}(\mathbf{r})=\int d^3r_1\,\Gamma_d(\mathbf{r},\mathbf{r}_1)v_{\rm JF}(\mathbf{r},\mathbf{r}_1)\rho_1(\mathbf{r}_1) \tag{4.16}$$

with

$$\tilde{\Gamma}_d(\mathbf{r}_1,\mathbf{r}_2)\equiv[\tilde{\Gamma}*S_F](\mathbf{r}_1,\mathbf{r}_2)\ . \tag{4.17}$$

(b) The second term arises from the density derivative of $\Gamma_{dd}(\mathbf{r}_i,\mathbf{r}_j)$. Using diagrammatic arguments, one arrives at

$$V_H^{(2')}(\mathbf{r})=\tfrac{1}{2}\int d^3r_1\int d^3r_2\,\Gamma_d(\mathbf{r},\mathbf{r}_1)\rho_1(\mathbf{r}_1)X'_{dd}(\mathbf{r}_1,\mathbf{r}_2)\rho_1(\mathbf{r}_2)\Gamma_d(\mathbf{r},\mathbf{r}_2)$$
$$+\frac{\hbar^2}{16m}\int d^3r_1\int d^3r_2\,\Gamma_{dd}(\mathbf{r},\mathbf{r}_1)\{[D(1)+D(2)][\rho_2^F(\mathbf{r}_1-\mathbf{r}_2)-\rho_1(\mathbf{r}_1)\rho_1(\mathbf{r}_2)]\}\Gamma_{dd}(\mathbf{r},\mathbf{r}_2)\ . \tag{4.18}$$

(c) Finally, the third term comes from the appearance of the one-body density in the operator $D(i)$ in $t_{\rm JF}$ and $T_{\rm JF}$. These terms can be combined into

$$V_H^{(3')}(\mathbf{r})=\frac{\hbar^2}{8m\rho_1(\mathbf{r})}\int d^3r_1\,\nabla_{\mathbf{r}}([\rho_2(\mathbf{r},\mathbf{r}_1)-\rho_1(\mathbf{r})\rho_1(\mathbf{r}_1)]\cdot\nabla_{\mathbf{r}}\{\ln[1+\Gamma_{dd}(\mathbf{r},\mathbf{r}_1)]-N_{dd}(\mathbf{r},\mathbf{r}_1)\})$$
$$-\frac{\hbar^2}{8m\rho_1(\mathbf{r})}\int d^3r_1\nabla_{\mathbf{r}}\{[\rho_2^F(\mathbf{r},\mathbf{r}_1)-\rho_1(\mathbf{r})\rho_1(\mathbf{r}_1)]\cdot\nabla_{\mathbf{r}}\Gamma_{dd}(\mathbf{r},\mathbf{r}_1)\}\ . \tag{4.19}$$

In the further algebraic manipulations we use repeatedly the Euler-Lagrange equation. Also, arguments corresponding to the ones discussed in the derivation of $\Delta T_{\rm JF}$ [cf. Eq. (4.14)] are used to bring the generalized (local) Hartree potential into its final form

$$V_H(\mathbf{r})=\sum_{i=0}^{4}V_H^{(i)}(\mathbf{r})\ , \tag{4.20}$$

where $V_H^{(0)}$ is the bare Hartree potential given in Eq. (4.15), and

$$V_H^{(1)}=\int d^3r_1\,\Gamma_d(\mathbf{r},\mathbf{r}_1)v_C(|\mathbf{r}-\mathbf{r}_1|)\rho_1(\mathbf{r}_1)\ , \tag{4.21}$$

$$V_H^{(2)}=\frac{\hbar^2}{8m}\int d^3r_1\,|\nabla_{\mathbf{r}_1}X_{dd}(\mathbf{r},\mathbf{r}_1)|^2\rho_1(\mathbf{r}_1)\ , \tag{4.22}$$

$$V_H^{(3)}=\frac{\hbar^2}{8m}\int d^3r_1\,\nabla_{\mathbf{r}}\Gamma_d(\mathbf{r},\mathbf{r}_1)\cdot\nabla_{\mathbf{r}}X_{dd}(\mathbf{r},\mathbf{r}_1)\rho_1(\mathbf{r}_1)\ , \tag{4.23}$$

$$V_H^{(4)}=-\frac{\hbar^2}{2m}\int d^3r_1\Gamma_{dd}(\mathbf{r},\mathbf{r}_1)\{|\nabla_{\mathbf{r}}[1+\Gamma_{dd}(\mathbf{r},\mathbf{r}_1)]^{1/2}|^2+|\nabla_{\mathbf{r}_1}[1+\Gamma_{dd}(\mathbf{r},\mathbf{r}_1)]^{1/2}|^2\}\rho_1(\mathbf{r}_1)\ . \tag{4.24}$$

The derivations of the generalized Fock term are, compared to the Hartree term, relatively simple. Since we have retained only the simplest exchange loops which connect no more than two points, the Fock term has the form

$$\left.\frac{\delta[E_2+T_{\rm JF}]}{\delta\rho_1^F(\mathbf{r}_1,\mathbf{r}_2)}\right|_{\rm Fock}=-\frac{1}{\nu}V_F(\mathbf{r}_1,\mathbf{r}_2)\rho_1^F(\mathbf{r}_1,\mathbf{r}_2)\ , \tag{4.25}$$

where the subscript Fock indicates that the variational derivative is carried out only with respect to nondegenerate exchange loops. The derivation of a closed-form expression for $V_F(\mathbf{r}_1,\mathbf{r}_2)$ is again most conveniently performed using diagrammatic arguments. The arguments parallel exactly the derivation of the single-particle spectrum for the infinite system[15,16] and need not be repeated here. The final form is simple compared with the result of Refs. 15 and 16 since no "*cc* diagrams" are summed. One finds

$$\tilde{V}_F(\mathbf{r}_1,\mathbf{r}_2)=\tilde{\Gamma}'_{dd}(\mathbf{r}_1,\mathbf{r}_2)-\tfrac{1}{4}[H_1*\tilde{\Gamma}_{dd}+\tilde{\Gamma}_{dd}*H_1](\mathbf{r}_1,\mathbf{r}_2)\ , \tag{4.26}$$

where the second term originates from the variation of $T_{\rm JF}$. [See paper III for the diagrammatic definition of $\Gamma'_{dd}(\mathbf{r}_1,\mathbf{r}_2)$.] Using the Euler-Lagrange and the FHNC equations, expression (4.26) can be simplified to

$$\tilde{V}_F(\mathbf{r}_1,\mathbf{r}_2)=-\tfrac{1}{2}[S_F^{-1}*H_1*\tilde{\Gamma}_{dd}+\tilde{\Gamma}_{dd}*H_1*S_F^{-1}](\mathbf{r}_1,\mathbf{r}_2)\ . \tag{4.27}$$

This derivation completes the formal aspects of our work. It is worth noting that the Fock potential $V_F(\mathbf{r}_1,\mathbf{r}_2)$ is short ranged due to the inclusion of the RPA screening, which is implicit in the summation of the chain diagrams in the FHNC theory. With the generalized Hartree potential [(4.19)—(4.23)] and the corresponding Fock term (4.26), the equation for the optimized single-particle basis is

$$\left[-\frac{\hbar^2}{2m}\nabla^2+U_{\text{ext}}(\mathbf{r})+V_H(\mathbf{r})\right]\phi_i(\mathbf{r}) -\frac{1}{\nu}\int d^3r'\,V_F(\mathbf{r},\mathbf{r}')\rho_1^F(\mathbf{r},\mathbf{r}')\phi_i(\mathbf{r}')=e_i\phi_i(\mathbf{r})\ . \tag{4.28}$$

V. JELLIUM MODEL OF METAL SLABS

A. Numerical model and approximations

In this work we have chosen to consider metal slabs which are translationally invariant in the x-y plane and symmetric about $z=0$. The jellium model takes for the positive-charge background

$$\rho_+(z)=\begin{cases}\rho_0 & \text{if } -d/2<z<d/2\ ,\\ 0, & \text{elsewhere}\ .\end{cases} \tag{5.1}$$

The solution of the full generalized Hartree-Fock equation (2.21) would be very complicated: The single-particle wave functions are of the form

$$\phi_i(\mathbf{r})=\varphi_{i,q_{||}}(z)e^{i\mathbf{r}_{||}\cdot\mathbf{q}_{||}}\ , \tag{5.2}$$

where $\mathbf{r}_{||}$ and $\mathbf{q}_{||}$ are the coordinate and wave number parallel to the surface. An unpleasant feature of the full Hartree-Fock problem is that the perpendicular component $\varphi_{i,q_{||}}(z)$ of the wave function depends explicitly on the wave number $q_{||}$ parallel to the surface. The need of diagonalizing the Hartree-Fock equation separately for all of these wave numbers would not only increase the computational effort substantially, but also require the numerical computation of all phase-space integrals to fill the Fermi sea. We felt that this would lead to unnecessary additional numerical uncertainties. Therefore we have resorted to an approximate treatment of the Fock term, originally suggested by Talman and Shadwick.[17] This procedure generates approximate single-particle states by a *local* one-body equation

$$\left[-\frac{\hbar^2}{2m}\nabla^2+U(\mathbf{r})\right]\phi_i(\mathbf{r})=\epsilon_i\phi(\mathbf{r})\ , \tag{5.3}$$

where the effective one-body potential is calculated by minimization of the *total* ground-state energy, i.e., by solving the equation

$$\frac{\delta E[U]}{\delta U(\mathbf{r})}=0\ . \tag{5.4}$$

The simplification has the immediate consequence that, due to our geometry, the effective one-body potential depends only on z, and the single-particle wave functions have the form

$$\phi_i(\mathbf{r})=\varphi_i(z)e^{i\mathbf{r}_{||}\cdot\mathbf{q}_{||}}\ . \tag{5.5}$$

The general derivation of the procedure may be found in Ref. 17, details of the implementation for our geometry will be given in Appendix C. Additional credibility to this approximate treatment of the Fock term will be drawn *a posteriori* from the fact that the nonlocalities contribute only a relatively small correction to the total one-body potential, i.e., the local Hartree-potential $V_H(z)$ and the effective potential $U(z)$ differ only by about 10%.

The equations were solved as follows: Let

$$U(z)=V_H^{(0)}(z)+\Delta V_H(z)+V_{\text{TS}}(z) \tag{5.6}$$

with

$$\Delta V_H(z)=\sum_{i=1}^{4}V_H^{(i)}(z)\ . \tag{5.7}$$

$V_{\text{TS}}(z)$ is the correction to the one-body potential induced by the exchange terms.

Starting at $r_s=1$ from a reasonable guess[18] for the one-body density, we set $\Delta V_H(z)=V_{\text{TS}}(z)=0$ and solve the Hartree equation (5.3). The so-called imaginary timestep method[19] proved to be an efficient and stable algorithm for this purpose. Using $V_{\text{p-h}}(\mathbf{r}_1,\mathbf{r}_2)\approx v_C(|\mathbf{r}_1-\mathbf{r}_2|)$ as an initial guess, we then solve the PPA equation (3.7). The solution of this equation allows us to compute a new estimate for the particle-hole interaction $V_{\text{p-h}}(\mathbf{r}_1,\mathbf{r}_2)$ [cf. Eq. (39)], the components $V_H^{(i)}$ $(i=1,2,3,4)$ [Eqs. (4.21)—(4.24)], and the Fock term (4.27). The correction $V_{\text{TS}}(z)$ can then be calculated by the averaging procedure described in Appendix C. Using $\Delta V_H(z)+V_{\text{TS}}(z)$ as a fixed external potential, the Hartree equation (5.2) is solved again and the procedure is repeated until convergence is reached. This first solution can then be taken as an initial estimate for solutions at different r_s values and film sizes d. Since we have decreased the density in rather small steps of r_s, the convergence is excellent; stable energies are typically reached within three to six iterations.

For comparison, we have used the same method to solve the uncorrelated Hartree-Fock equations, i.e., the corresponding one-body equations with $V_H^{(i)}=0$ for $1\le i\le 4$ and

$$V_F(\mathbf{r}_1,\mathbf{r}_2)=v_C(|\mathbf{r}_1-\mathbf{r}_2|)\ .$$

Calculations were performed for a number of metals of physical interest in the range $2.07\le r_s\le 5.23$: Al, Pb, Mg, Li, Na, K, and Rb.

B. Energies, densities, and one-body potentials

We have solved the coupled FHNC—Euler-Lagrange—Hartree-Fock equations for each of the above-mentioned materials for slab dimensions $d=8a_0r_s$, $10a_0r_s$, $12a_0r_s$, and $14a_0r_s$ (a_0 is the Bohr radius). From the ground-state energy as a function of the slab width d and hence, the particle number n, we can obtain by extrapolation

TABLE I. Ground-state energies for different slab dimension d for a variety of metals. The $d=\infty$ results are extrapolated from the finite slab results as described in the text. All energies are given in rydbergs. The second entry in each row is the corresponding correlation energy E_c. The numbers in parentheses in the last column are results from the bulk FHNC//0 calculation described in Appendix A.

		d ($r_s a_0$)				
r_s	Metal	8	10	12	14	∞
2.07	Al	−0.009 25	−0.008 93	−0.008 79	−0.008 69	−0.0079 (−0.0070)
		−0.075 19	−0.076 59	−0.077 35	−0.077 84	−0.0814 (−0.0801)
2.30	Pb	−0.055 84	−0.056 01	−0.056 22	−0.056 38	−0.0571 (−0.0563)
		−0.070 87	−0.072 33	−0.073 07	−0.073 55	−0.0771 (−0.0757)
2.66	Mg	−0.099 06	−0.099 71	−0.100 23	−0.100 60	−0.1027 (−0.1021)
		−0.065 36	−0.066 66	−0.067 39	−0.067 84	−0.0711 (−0.0699)
3.28	Li	−0.131 24	−0.132 23	−0.132 95	−0.133 46	−0.1364 (−0.1360)
		−0.057 85	−0.058 89	−0.059 63	−0.060 05	−0.0630 (−0.0620)
3.99	Na	−0.140 77	−0.141 83	−0.142 61	−0.143 15	−0.1463 (−0.1459)
		−0.051 31	−0.052 08	−0.052 88	−0.053 27	−0.0556 (−0.0551)
4.96	K	−0.137 86	−0.138 90	−0.139 64	−0.140 11	−0.1431 (−0.1409)
		−0.044 56	−0.045 25	−0.045 92	−0.046 25	−0.0486 (−0.0480)
5.23	Rb	−0.135 76	−0.136 83	−0.137 32	−0.137 49	−0.1398 (−0.1407)
		−0.042 96	−0.043 68	−0.044 17	−0.044 44	−0.0464 (−0.0463)

$$2\sigma_u = E[n] - E_\infty n \tag{5.8}$$

both a surface energy σ_u and a bulk energy E_∞. The asymptotic energy E_∞ should agree with the energy obtained in an independent calculation of the homogeneous electron gas. This is an important test for the numerical accuracy since calculations for the bulk system can be done on a much finer mesh.

Table I shows our energies per particle for the above-mentioned materials and slab dimensions. The asymptotic energy E_∞ has been obtained by a linear fit of these data. Also shown are correlation energies E_c, cf. Eq. (4.9), the extrapolated values E_∞ and the corresponding bulk energies obtained in the calculation described in Appendix A. We see that the extrapolated and the calculated bulk energies agree within about 1%, which lends credibility to our numerical treatment. (The case of Al is exceptional since the total energy results from large cancellations between kinetic, Coulomb, exchange, and correlation energy. A comparison of the extrapolated and the bulk correlation energy gives a more realistic estimate of the numerical accuracy.)

Slight deviations from a linear behavior of the ground-state energy are caused by the fact that the number of occupied orbitals $\varphi_i(z)$ changes. This induces an uncertainty in the surface energy. We have estimated this uncertainty by calculating the surface energy independently for each slab dimension d from the extrapolated ground-state energy E_∞. An error estimate is then obtained from

$$\Delta\sigma_u = \tfrac{1}{2}\{\langle [E(n) - E_\infty n]^2 \rangle\}^{1/2} . \tag{5.9}$$

Consistent with our approximation of the FHNC equations, the one-body density $\rho_1(\mathbf{r})$ is simply the Hartree density derived from the single-particle wave functions $\phi_i(\mathbf{r}_j)$. While the identification is not exact, we have eliminated large classes of corrections by the optimal choice of the single-particle basis and the one-body function $u_1(\mathbf{r})$. The density profiles are shown, for the slabs of $14 a_0 r_s$ thickness, in Fig. 6. The density profiles in the vicinity of the jellium edge do not change noticeably with the thickness of the slab.

Figure 7(a) shows, for potassium ($r_s = 4.96$), a comparison of our density profile with the one obtained by Lang and Kohn[20] at $r_s = 5$. We find that in our calculation the first peak of the density is somewhat less pronounced than

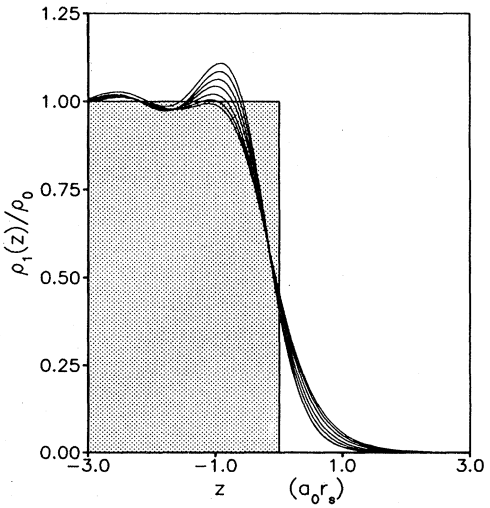

FIG. 6. The one-body density $\rho_1(\mathbf{r})$ is shown for Rb, K, Na, Li, Mg, Pb, and Al. The density with the largest peak corresponds to Rb, the one with the smallest peak to Al. The shaded area is the jellium background. All densities are from calculations for the slab dimension $d = 14 a_0 r_s$. Coordinates are chosen such that $z = 0$ at the jellium edge.

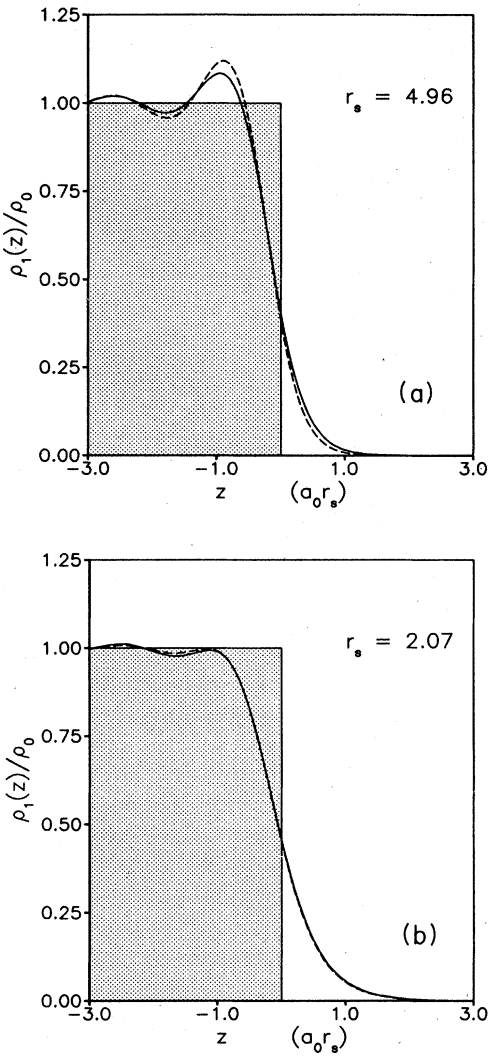

FIG. 7. (a) Our one-body density for K ($r_s=4.96$) (solid line) is compared with the Lang-Kohn result for $r_s=5$ (dashed line). The shaded area is the jellium background. (b) Our one-body density for Al ($r_s=2.07$) (solid line) is compared with the Lang-Kohn result for $r_s=2$ (dashed line). The shaded area is the jellium background.

the one found by Lang and Kohn. The difference in the DF profiles and ours decreases with increasing density. At $r_s=2.07$, our density is virtually indistinguishable from the Lang-Kohn density at $r_s=2$, cf. Fig. 7(b).

Figure 8 shows, for aluminum, the decomposition of the one-body potential into the Hartree term $V_H^{(0)}(z)$ of Eq. (4.15), the full local-one-body potential $V_H(z)$ of Eq. (4.20), and the local potential correction $V_{TS}(z)$ induced by the exchange term $V_F(\mathbf{r}_1,\mathbf{r}_2)$. We see that the pair correlations have a substantial effect on the local-one-body potential; the Hartree term is enhanced by about a factor of 2. On the other hand, the nonlocalities play a rather small role; they add only a 10% correction to the local generalized Hartree potential $V_H(z)$. Figure 9 shows these potentials for potassium; the situation is very similar

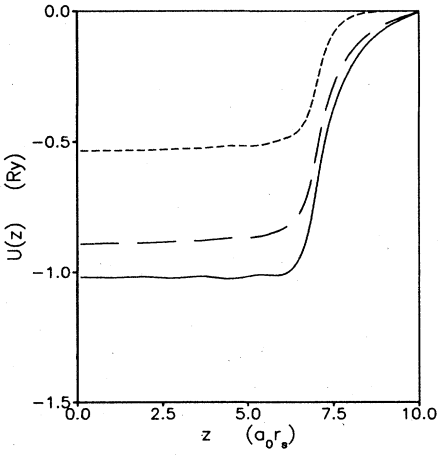

FIG. 8. The composition of the full one-body potential $U(z)$, Eq. (5.6) (solid line), from the electrostatic potential $V_H^{(0)}(z)$ (short-dashed line), generalized Hartree-potential $V_H(z)$, Eq. (4.20) (long-dashed line), is shown for aluminum. The jellium edge is at $z=7a_0r_s$.

for the other materials.

The comparison of the full one-body potential with the one obtained in Hartree-Fock approximation is quite interesting (Fig. 10). Due to the absence of the RPA screening, the induced term $V_{TS}(z)$ is much larger, whereas the Hartree term remains essentially the same, and the total optimized one-body potential changes very little.

These jellium-model surface energies as calculated by the extrapolation outlined above are shown in Table II. We show also the results obtained by Lang and Kohn[20] and by Sun *et al.*[8] Other calculations are worth noting: the work of Monnier and Perdew[21] and Sahni *et al.*[22] We will restrict our comparisons to the work of Refs. 8 and 20: The Lang-Kohn theory is the first calculation of this kind, and the work of Ref. 8 is most closely related to ours. We find that our jellium surface energies are, except for $r_s=2.07$ and $r_s=2.3$, somewhat above the results of Refs. 20 and 8.

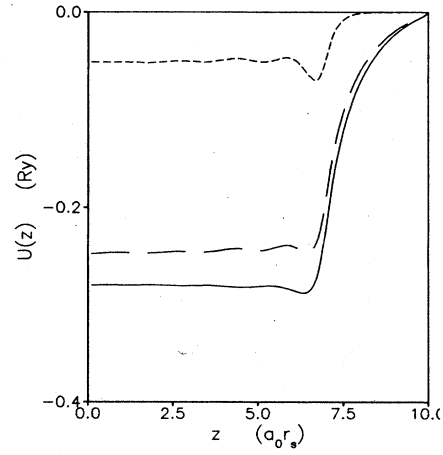

FIG. 9. Same as Fig. 8 for potassium.

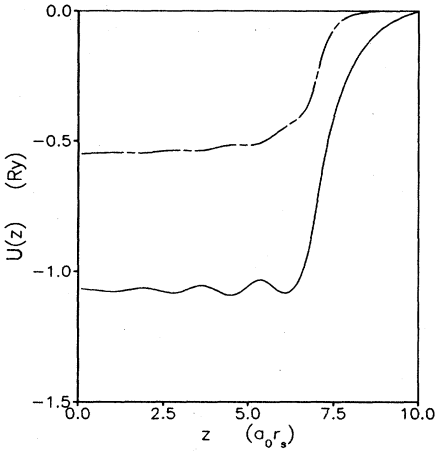

FIG. 10. The one-body potential $U(z)$ in the Hartree-Fock approximation (solid line) and the electrostatic potential (dashed line) are shown for aluminum. The jellium edge is at $z=7a_0r_s$.

TABLE II. Comparison of the surface energies obtained for the jellium model by Lang and Kohn (Ref. 20), column 3, Sun *et al.* (Ref. 9), column 4, and in the present work in the jellium-background model (FHNC//0, column 5). All surface energies are given in ergs/cm^2. The error estimates are generated by comparing the surface energy predicted by each individual calculation when compared with the *extrapolated* bulk energy (column 6 in Tables I and II).

r_s	Metal	LK	SFW	FHNC//0
2.07	Al	−730	102	−222±5.0
2.30	Pb	−130	278	181±6.0
2.66	Mg	110	309	383±3.0
3.28	Li	210	363	360±1.6
3.99	Na	160	204	261±1.2
4.96	K	100	94	159±0.6
5.23	Rb	85	76	105±3.9

C. Pair distributions and correlation functions

One of the major objectives of our calculations is to obtain information on the importance of density-dependent and anisotropic correlations. The most obvious quantity to study in this connection is the pair-distribution function $g(\mathbf{r},\mathbf{r}')$. We have used in this work the expression

$$\rho_2(\mathbf{r},\mathbf{r}')=[1+\Gamma_{dd}(\mathbf{r},\mathbf{r}')]\{\rho_2^F(\mathbf{r},\mathbf{r}')+[\rho_1(\mathbf{r})\rho_1(\mathbf{r}')]^{1/2}[S_F*\tilde{\Gamma}_{dd}*S_F-\tilde{\Gamma}_{dd}](\mathbf{r},\mathbf{r}')\}\ , \tag{5.10}$$

$$g(\mathbf{r},\mathbf{r}')=\frac{\rho_2(\mathbf{r},\mathbf{r}')}{\rho_1(\mathbf{r})\rho_1(\mathbf{r}')}\ . \tag{5.11}$$

The expression is derived from the static form factor $S(\mathbf{r},\mathbf{r}')$ [Eq. (3.6)] by adding, after Fourier transform, all those diagrams that are missing in (3.6) to obtain the common factor $1+\Gamma_{dd}(\mathbf{r},\mathbf{r}')$, but which would violate the correct long-wavelength behavior of the static form factor unless higher-order "elementary" diagrams are included.[9,14]

The coordinate system in which the anisotropy of the pair correlation function is minimal is the one where the center of mass of the two particles is fixed at a certain distance $z_{\text{c.m.}}=(z_1+z_2)/2$ from the center of slab, and the pair correlation function is considered as a function of the distance $r_{||}$ of the two particles parallel and $|z_1-z_2|$ perpendicular to the surface. In the center of the slab, one should expect bulk behavior and a comparison of the pair-distribution function with the corresponding bulk distribution function gives an estimate for the numerical accuracy of the calculation. This comparison is shown, for the Al slab of $d=14a_0r_s$, in Fig. 11. The agreement is shown to be excellent, the pair-distribution function is isotropic within drawing accuracy. The situation for the other materials is identical.

Anisotropies are to be expected in the vicinity of the surface. We show in Figs. 12(a)–12(c) the pair-distribution function for two particles located at about $0.61a_0r_s$ inside the jellium edge, on the jellium edge, and $0.61a_0r_s$ outside the jellium edge. Comparison is made with the local-density approximation obtained by interpolation from the bulk electron-gas calculations. We see that anisotropies can be larger then 10% and the deviation from the local-density approximation is of the same order of magnitude. In particular, in the low-density regime, the local-density approximation fails severely. Our results

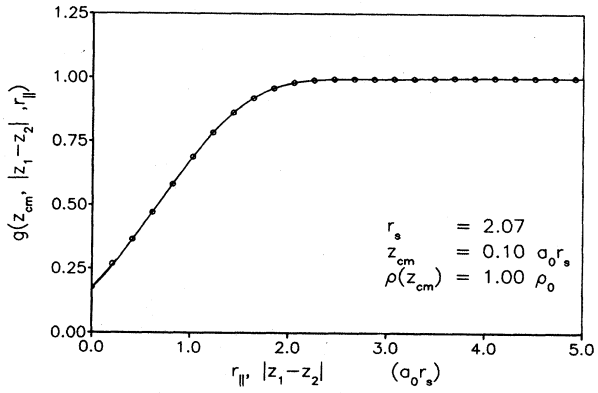

FIG. 11. The pair-distribution function $g(z_1,z_2,r_{||})$ for aluminum is shown for a pair of particles having the center-of-mass coordinate $z_{\text{c.m.}}$ close to the center of the slab. The values of the pair-distribution function parallel and perpendicular to the surface are indistinguishable. The circles indicate that the results from a bulk calculation at the same density.

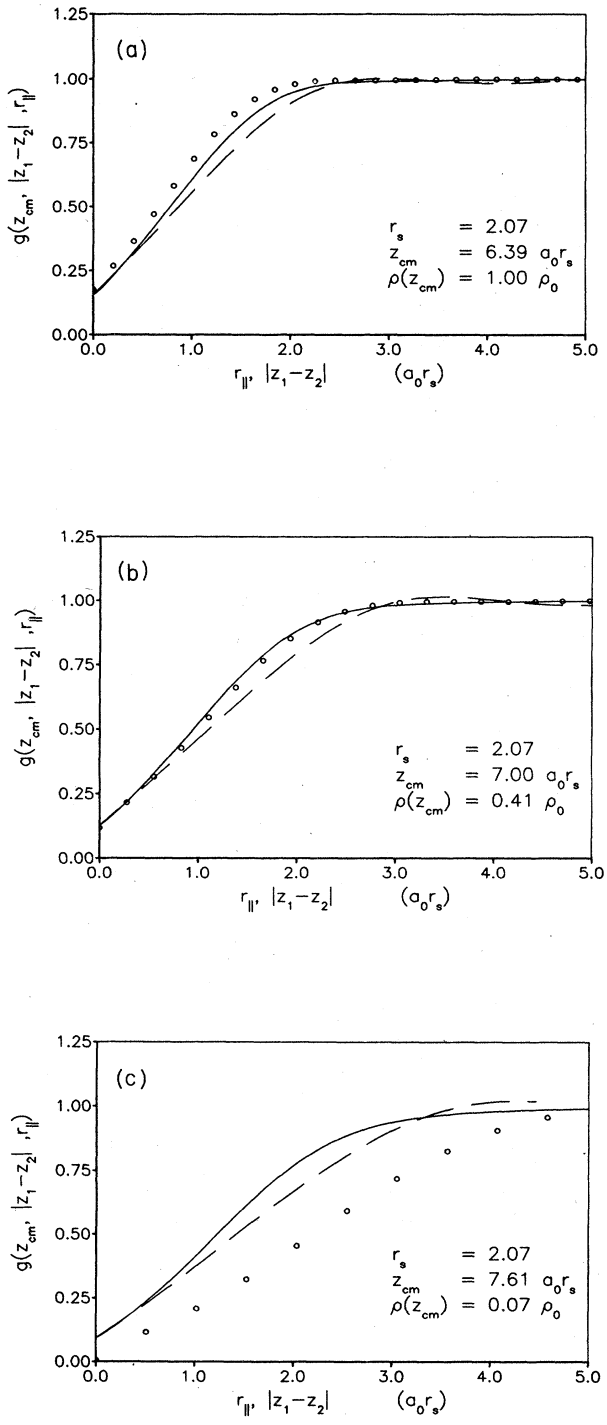

FIG. 12. (a) The pair-distribution function $g(z_1,z_2,r_{||})$ is shown in aluminum, for a pair of particles having the center-of-mass coordinate $z_{c.m.}$ close to the jellium edge inside the slab, as a function of $r_{||}$ for $|z_1-z_2|=0$ (solid line) and as a function of $|z_1-z_2|$ for $r_{||}=0$ (dashed line). The local density at the center of mass is equal to the central density ρ_0. The circles indicate the results from a bulk calculation at the same density $\rho_1(z_{c.m.})$. (b) Same as (a) for a pair of particles having their center of mass $z_{c.m.}$ on the jellium edge. (c) Same as (a) for a pair of particles having their center of mass $z_{c.m.}$ slightly outside the jellium edge.

are very similar for other materials; as another example we show in Figs. 13(a)—13(c) the corresponding pair-distribution functions for potassium.

The anisotropy of the pair distribution function is displayed more clearly in a coordinate system, where one particle is held fixed. We show in Fig. 14 for aluminum, a contour plot of the pair-distribution function $g(z_1,z_2,r_{||})$ for two particles, one of which is held at the jellium edge.

In view of further applications of the optimal correlation functions calculated in our work, for example, in a more accurate Monte Carlo evaluation of the energy-

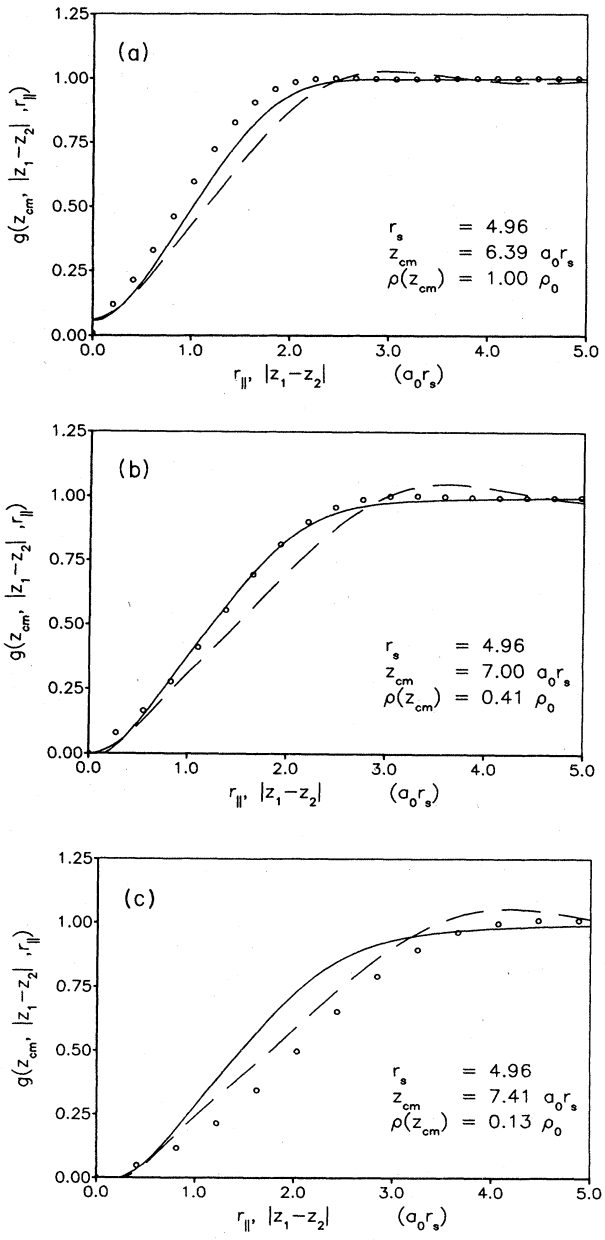

FIG. 13. (a) Same as Fig. 12(a) for potassium. (b) Same as Fig. 12(b) for potassium. (c) Same as Fig. 12(c) for potassium.

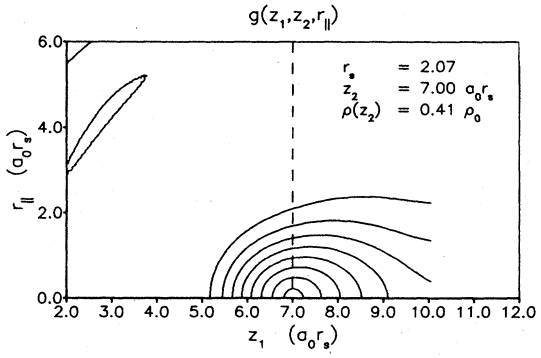

FIG. 14. For an electron located in Al at the jellium edge (i.e., z_2 is kept fixed), we show the lines of constant $g(z_1,z_2,r_{||})$. The contours correspond to $g(z_1,z_2,r_{||})=0.2,0.3,\ldots,0.9$.

expectation value, it is also interesting to study the pair correlation function

$$f^2(\mathbf{r}_1,\mathbf{r}_2)\equiv\exp[u_2(\mathbf{r}_1,\mathbf{r}_2)] .$$

We have seen above that both the local-density approximation and the assumption of isotropy for the pair-distribution function $g(\mathbf{r}_1,\mathbf{r}_2)$ fail in the surface. The approximations made in earlier variational work on inhomogeneous systems have been even more severe: Generally, the pair correlation function $\exp[u_2(\mathbf{r}_1,\mathbf{r}_2)]$ has been assumed to be a density-independent, isotropic function throughout the system. These assumptions can be easily tested within our theory. For given $N_{dd}(\mathbf{r}_1,\mathbf{r}_2)$ and $\Gamma_{dd}(\mathbf{r}_1,\mathbf{r}_2)$, we obtain from Eqs. (3.2) and (3.5)

$$f^2(\mathbf{r}_1,\mathbf{r}_2)=[1+\Gamma_{dd}(\mathbf{r}_1,\mathbf{r}_2)]\exp[-N_{dd}(\mathbf{r}_1,\mathbf{r}_2)] . \quad (5.12)$$

We show in Fig. 15, for K and the slab dimension $14a_0r_s$, the pair correlation function $f^2(\mathbf{r}_1,\mathbf{r}_2)$ in the center of the slab and on the jellium edge. Comparison is made between the values of this function in different directions, and the bulk correlation function at the corresponding lo-

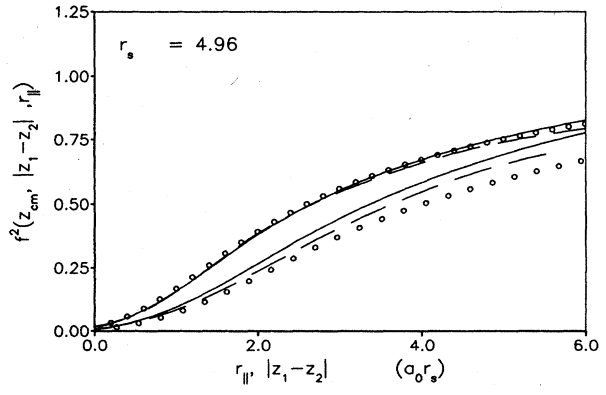

FIG. 15. The upper three curves show, for potassium, the pair correlation function $f^2(z_{\text{c.m.}},|z_1-z_2|,r_{||})$ for a pair of particles with their center of mass $z_{\text{c.m.}}$ in the center of the slab, parallel (solid line) and perpendicular (dashed line) to the surface. The circles indicate the corresponding bulk correlation function. The lower three curves show the same comparison for a pair of particles whose center of mass is on the jellium edge.

cal density. We see that the anisotropy and density dependence is less pronounced than for the distribution functions. But the correlation function in the surface deviates notably from the one in the center of the slab. Whereas local-density or isotropic approximations for the pair correlation functions might be considered acceptable, the assumption of density independence of the correlation function is certainly not. The situation is very similar for other values of r_s.

D. Remarks on lattice corrections and work functions

The jellium model is an idealized model of a real metal. As was first studied by Lang and Kohn,[20] there are large corrections to the surface energy of a metal due to existence and nonuniformity of the ion-lattice background. Lang and Kohn have estimated the size of the lattice corrections by first-order perturbation theory, using averaged pseudopotentials originally suggested by Ashcroft.[21] Later improvements of that by Monnier and Perdew[22] and by Sahni *et al.*[23] included somewhat better estimates of the effects of the nonuniform background potential and the relaxation of the first lattice plane. Monnier and Perdew[22] have pointed out that the nonuniform background potential can cause, especially for lead, significant changes of the electron density. This makes an estimate of lattice corrections by first-order perturbation theory questionable. In fact, the potential correction term $\delta v(z)$ is *not* small compared with the effective one-body potential $U(z)$. Monnier and Perdew have therefore included background effects in a variational, but averaged way. Since our present approach does not make any assumption on the form of the background potential, it is easy to implement a one-dimensional oscillating potential $\delta v(z)$ in the generalized Hartree-Fock equation (2.21). But it turns out that the full inclusion of the background potential induces unrealistically large density fluctuations (up to 25% for lead). Therefore, we felt that the question of the nonuniformity of the ion background involves considerations quite distinct from the problem of describing the electrons adequately and have decided, for the sake of comparison, but aware of the deficiencies, to use the Lang-Kohn first-order approximation.

To include the lattice corrections, we follow the route of Ref. 20, which leads to two correction terms to the surface energy, (a) the classical cleavage energy σ_{cl} and (b) the energy

$$\delta\sigma_{ps}=\int_0^\infty \delta v(z)[\rho(z)-\rho_+(z)] \quad (5.13)$$

caused by the direct modification of the electron density due to a nonuniform background potential $\delta v(z)$. The analytic form of the potential correction $\delta v(z)$ may be found in Appendix D of Ref. 20.

The cleaving energy σ_{cl} is independent of the electronic structure of the metal; we can take here the results of Ref. 20 and their extensions by Monnier and Perdew[22] and Sahni *et al.*[23] The correction term σ_{ps} caused by the nonuniform background potential is calculated using the one-electron density of the jellium model. The decomposition of the total surface energy into the jellium contribution, the classical cleavage energy, and the background

TABLE III. Composition of the total surface energies $\sigma=\sigma_u+\delta\sigma_{\rm cl}+\delta\sigma_{ps}$ in the ion-lattice model into the jellium-model contribution σ_u, the classical cleavage energy $\delta\sigma_{\rm cl}$, and the lattice-correction term $\delta\sigma_{ps}$. The values for $\delta\sigma_{\rm cl}$ were taken from Refs. 20, 22, and 23. All surface energies are given in ergs/cm^2.

r_s	Metal	Face	σ_u	$\delta\sigma_{ps}$	$\delta\sigma_{\rm cl}$	σ
2.07	Al	(111)	−222	1136	409	1323
2.30	Zn	(0001)	181	580	99	860
2.30	Pb	(111)	181	1159	397	1737
2.66	Mg	(0001)	383	296	131	810
3.28	Li	(110)	360	134	59	553
3.99	Na	(110)	261	24	33	318
4.96	K	(110)	159	12	17	188
5.23	Rb	(110)	105	−1.0	15	119

correction is shown in Table III; a comparison of our results with those of Refs. 8 and 20 and experimental work[24–29] is given in Table IV.

Our surface energies are in all cases higher than the experimental values, and also higher than all previously published results. The discrepancy is especially pronounced in lead. We attribute most of this to the missing relaxation to the nonuniform background. We note also that the correction $\delta\sigma_{ps}$ is a rather sensitive functional of the one-body density since the net energy correction is to the cancellation of large positive and negative terms.

As for the lattice corrections, we adopt also for the calculation of the work function the Lang-Kohn procedure.[30] There, the work function is given by

$$\phi=\Phi_u-\mu-\langle\delta\Phi\rangle\ , \tag{5.14}$$

where μ is the bulk chemical potential,

$$\mu=\frac{d(nE/A)}{dn}\ . \tag{5.15}$$

In our case of a slab geometry of finite dimension, we have

$$\Phi_u=V_H^{(0)}(\infty)-V_H^{(0)}(0)\ . \tag{5.16}$$

This identification is justified if the electrostatic potential is sufficiently constant inside the slab. $\langle\delta\Phi\rangle$ is a lattice correction term[30] which needs an independent calculation of the change of the one-body density if one particle is removed. The correction term is relatively small in the Lang-Kohn work and depends also on details of the nonuniform background potential. In view of our above considerations we postpone the study of these corrections until the background corrections are included in a more self-consistent way.

The bulk chemical potential can be obtained via Eq. (5.15) from the bulk correlation energy. Here we have followed a procedure adopted by Ceperley,[31] who makes a global Padé approximation to the correlation energy per particle as a function of r_s:

$$E_c/A=\frac{a}{1+\beta_1 r_s^{1/2}+\beta_2 r_s}\ . \tag{5.17}$$

We have adopted the same analytic form for our FHNC//0 results and calculated the chemical potential for both the variational Monte Carlo results of Ref. 31 and our bulk FHNC calculation. The Coulomb barrier can be obtained from the variational calculations for the inhomogeneous system. Results and a comparison with the calculations of Refs. 8 and 30 and the experimental data of Ref. 29 are shown in Table V. Again we see that the jellium-model work functions are throughout noticeably above those of earlier calculations.

TABLE IV. Comparison of the theoretical predictions for the surface energy as given by Lang and Kohn (LK, Ref. 20), Sun *et al.* (SWF, Ref. 9), and FHNC//0. The experimental values are minimum and maximum values found in Refs. 24–29. All energies are given in ergs/cm^2.

r_s	Metal	Face	LK	SFW	FHNC//0	Expt.
2.07	Al	(111)	730	977	1323	965–1170
2.30	Zn	(0001)	480	547	860	350–1040
2.30	Pb	(111)	1140	1118	1737	593–690
2.66	Mg	(0001)	546	672	810	712–785
3.28	Li	(110)	380	465	553	470–522
3.99	Na	(110)	230	264	318	220–275
4.96	K	(110)	140	124	188	125–145
5.23	Rb	(110)	120	107	119	95–117

TABLE V. Electron-gas chemical potentials obtained from the variational Monte Carlo equation of state (column 3) and the FHNC//0 equation of state (column 4). Column 5 shows the dipole barrier obtained in our calculation, and column 6 the jellium-model work function. Columns 7 and 8 give the corresponding results of Refs. 30 and 9. (The results of Ref. 9 include the lattice correction.) Column 9 quotes the experimental results of Ref. 29. All energies are given in eV.

Metal	r_s	μ_{MC}	μ_{FHNC}	$\Delta\Phi$	Φ_{FHNC}	LK	SFW	Expt.
Al	2.07	2.30	2.39	7.29	4.90	3.87	3.6	4.19
Zn	2.30	0.94	1.03	5.84	4.81	3.80	3.0	4.33
Mg	2.66	−0.39	−0.30	4.08	4.38	3.66	3.0	3.66
Li	3.28	−1.52	−1.42	2.40	3.92	3.37	3.6	3.1
Na	3.99	−2.03	−1.93	1.43	3.36	3.06	2.9	2.7
K	4.96	−2.22	−2.11	0.72	2.83	2.74	2.7	2.39
Rb	5.23	−2.23	−2.11	0.61	2.72	2.63	2.2	2.21

VI. SUMMARY

In this paper we have presented results of what we consider to be at present, the most advanced application of microscopic many-body theory to large inhomogeneous systems. It is the first application of the optimized FHNC theory for an inhomogeneous problem. The theory contains no adjustable parameters; the only approximations are the form of the correlated wave function and the level of FHNC approximation. The correlated wave function (1.1) has proved[31] to be an excellent choice for homogeneous electronic systems. The FHNC//0 approximation causes some additional uncertainties, but it is also quite satisfactory for the bulk electron gas. The use of more sophisticated FHNC approximations (such as the FHNC/C approximation of Ref. 14) would increase the computational effort by about a factor of 2, in other words it is quite feasible. But experience from studies of homogeneous systems[9,14] suggests that the higher-order correction terms are rather random in nature, and that the basic physics is described correctly within the FHNC//0 approximation.

The results of our calculations are, nevertheless, somewhat disturbing in the sense that they produce higher values for the jellium surface energy and the work function than expected. A possible source of uncertainty is the approximation $\rho_1(\mathbf{r})\approx\rho_1^F(\mathbf{r})$, which is the only one that has not yet been tested. The need for cluster expansions for the one-body density is a new feature of theories of inhomogeneous Fermi systems. One may investigate the accuracy of this approximation by calculating the first-order correction terms, i.e., the fourth and fifth diagram shown in Fig. 2. However, instead of going beyond the FHNC//0 approximation and calculating some more sets of diagrams, we feel that it is more instructive to pursue immediately a Monte Carlo evaluation of the energy and the densities using our optimized correlation functions. Such a calculation is under way. The jellium model, which does not suffer from the uncertainties of the inhomogeneous ion lattice background, is a sufficiently well-defined system and will allow conclusive comparisons.

Only slight rearrangements of the algorithm used here allow the same method to be used for the surface of liquid ^{3}He or adsorbed films. Spherical systems can be treated in a very similar way, though the flat-surface geometry is computationally more efficient. With the proper extension of the optimized FHNC theory to state-dependent correlations finally in sight,[32] we believe that microscopic calculations for finite nuclei will also be feasible in the foreseeable future.

ACKNOWLEDGMENTS

This work was supported, in part, by the Deutsche Forschungsgemeinschaft (E.K.) and by the National Science Foundation under Grants No. DMR-81-14556 and No. PHY-77-27804, supplemented by funds from the U.S. National Aeronautics and Space Administration, as well as by the U.S. Office of Naval Research under Contract No. N00014-82-K-0626. Computing resources were provided by the Department of Physics and by the College of Academics and Research at Texas A&M University, as well as by the Institute for Theoretical Physics and by the Department of Physics at the University of California, Santa Barbara. One of us (E.K.) wishes to thank R. A. Smith for discussions and helpful suggestions.

APPENDIX A: BULK ELECTRON-GAS CALCULATION

We give in this appendix the bulk limit of the FHNC//0 and Euler-Lagrange equations used in our work, and present numerical results for that approximation. For a description of the full FHNC/C procedure in electronic systems, the reader is referred to Ref. 14. In that paper, all diagrams had been summed that can be summed with two-body equations, and estimates for higher-order exchange diagrams were included to all orders. To avoid an excessive computational effort, the present work has employed the simplest version of the FHNC theory. The FHNC and the Euler-Lagrange equations for the bulk electron gas assume the form

$$S(k)=\frac{S_F(k)}{[1+(4m\rho/\hbar^2k^2)S_F^2(k)\tilde{V}_{\text{p-h}}(k)]^{1/2}}\ , \tag{A1}$$

where

$$S_F(k)=\begin{cases}3k/4k_F-k^3/16k_F^3, & k<2k_F\\ 1, & k\geq 2k_F\end{cases} \tag{A2}$$

is the static form factor of the noninteracting Fermi system. The particle-hole interaction $V_{\text{p-h}}(r)$ has the form

$$V_{\text{p-h}}(r)=[1+\Gamma_{dd}(r)]v_C(r)$$
$$+\frac{\hbar^2}{m}\,|\,\nabla[1+\Gamma_{dd}(r)]^{1/2}\,|^2+\Gamma_{dd}(r)w_I(r)\ , \quad \text{(A3)}$$

and Γ_{dd} is related to the static form factor $S(k)$ through

$$S(k)=S_F(k)+S_F^2(k)\tilde{\Gamma}_{dd}(k)\ . \quad \text{(A4)}$$

The tilde denotes the dimensionless Fourier transform

$$\tilde{f}(k)\equiv\rho\int d^3r\,f(r)\exp(i\mathbf{k}\cdot\mathbf{r})\ . \quad \text{(A5)}$$

Finally, the "induced interaction" $w_I(r)$ is of the form

$$\tilde{w}_I(k)=-\frac{\hbar^2k^2}{4m}\left[1+2\frac{S(k)}{S_F(k)}\right]\left[\frac{1}{S(k)}-\frac{1}{S_F(k)}\right]^2\ . \quad \text{(A6)}$$

Equations (A1)—(A6) form a closed set which allows the calculation of the static form factor $S(k)$ from the bare Coulomb potential $v_C(r)$. From an initial guess of the particle-hole interaction $V_{\text{p-h}}(r)$ one computes via Eq. (A1) the static form factor and from Eqs. (A2) and (A4) the quantities $\Gamma_{dd}(r)$ and $w_I(r)$. These are used in Eq. (A3) to compute a new particle-hole interaction, and the process is repeated until convergence is reached. At high densities $r_s\leq 1$ it is sufficient to start with the bare Coulomb potential, at lower densities one can use one of the higher-density results as a starting point of the iterations. Depending on the density, convergence is reached after 3—10 iterations. The procedure works more efficiently than in systems with a hard-core interaction, since no precautions need to be made to maintain a proper short-ranged behavior of $\Gamma_{dd}(r)$.

Once a numerical solution of the Euler-Lagrange equations is obtained, the energy can be calculated via Eqs. (4.9), (4.10), (4.13), and (4.14). For the homogeneous system, these expressions assume the simple form

$$\Delta E_{\text{pot}}/A=\frac{1}{2\rho}\int\frac{d^3k}{(2\pi)^3}[S(k)-S_F(k)][\tilde{v}_C(k)-\tilde{V}_{\text{p-h}}(k)]\ , \quad \text{(A7)}$$

$$E_{\text{RPA}}/A=\frac{\hbar^2}{8m\rho}\int\frac{d^3}{(2\pi)^3}k^2\frac{[S(k)-S_F(k)]^2}{S^2(k)S_F(k)}\ , \quad \text{(A8)}$$

TABLE VI. Comparison of the correlation energy of the bulk electron gas as obtained from the variational Monte Carlo calculations of Ref. 31 (MC, column 2), in the random-phase approximation (RPA, column 3), in the FHNC/C calculation of Ref. 14 (column 4) and in the present FHNC//0 approximation (column 5) as a function of r_s (column 1). All energies are given in rydberg units.

r_s	MC	RPA	FHNC/C	FHNC//0
1.0	−0.122	−0.158	−0.134	−0.113
2.0	−0.087	−0.124	−0.094	−0.082
3.0	−0.072	−0.106	−0.073	−0.065
4.0	−0.062	−0.094	−0.064	−0.055
5.0	−0.055	−0.085	−0.056	−0.048

$$\Delta T_{\text{JF}}/A=-\frac{\hbar^2\rho}{2m}\int d^3r\,\Gamma_{dd}(r)\,|\,\nabla[1+\Gamma_{dd}(r)]^{1/2}\,|^2\ . \quad \text{(A9)}$$

The results of the simplified FHNC/EL calculation are shown in Table VI in comparison with the Green's-function Monte Carlo results of Ceperley and Alder,[3] the random-phase approximation (RPA), and the full FHNC/C treatment of Ref. 14. The simplified FHNC treatment is not quite as good as the full FHNC/C calculation, especially at lower densities, but it compares favorably with the RPA, and the uncertainties in the bulk ground-state energy are likely to have no large effect on the surface energy. The decomposition of the correlation energy

$$E_c=\Delta E_{\text{pot}}+E_{\text{RPA}}+\Delta T_{\text{JF}} \quad \text{(A10)}$$

is shown in Table VII. We see that ΔE_{RPA} is dominant only at high densities.

APPENDIX B: NUMERICAL SOLUTION OF THE PPA EQUATION

Our algorithm for solving the PPA equation (3.7) is closely related to the normal-mode decomposition pro-

TABLE VII. Decomposition of the correlation energy of the bulk electron liquid in the FHNC//0 approximation as a function of r_s. All energies are given in rydberg units. The last two columns give the chemical potential derived from the FHNC//0 results (column 6) and from the variational Monte Carlo energies (Ref. 31).

r_s	E_{RPA}	ΔE_{pot}	ΔT_{JF}	E_c	μ_{FHNC}	μ_{MC}
2.00	−0.0592	−0.0388	0.0165	−0.0815	0.2141	0.2081
2.07	−0.0579	−0.0384	0.0162	−0.0801	0.1751	0.1690
2.30	−0.0540	−0.0371	0.0153	−0.0757	0.0755	0.0691
2.66	−0.0489	−0.0351	0.0141	−0.0699	−0.0219	−0.0287
3.00	−0.0450	−0.0333	0.0130	−0.0653	−0.0760	−0.0831
3.28	−0.0422	−0.0320	0.0122	−0.0620	−0.1044	−0.1117
3.99	−0.0367	−0.0290	0.0105	−0.0551	−0.1414	−0.1489
4.00	−0.0366	−0.0289	0.0105	−0.0550	−0.1417	−0.1492
4.96	−0.0313	−0.0255	0.0088	−0.0480	−0.1550	−0.1628
5.00	−0.0311	−0.0254	0.0087	−0.0478	−0.1551	−0.1629
5.23	−0.0301	−0.0247	0.0084	−0.0463	−0.1555	−0.1632

cedure developed in papers I and II for Bose systems. We use

$$\tilde{X}_{dd}(\mathbf{r}_1,\mathbf{r}_2)=S_F^{-1}(\mathbf{r}_1,\mathbf{r}_2)-S^{-1}(\mathbf{r}_1,\mathbf{r}_2) \tag{B1}$$

and rewrite Eq. (3.7) in the form

$$[S^{-1}*H_1*S^{-1}](\mathbf{r}_1,\mathbf{r}_2) =2\tilde{V}_{\text{p-h}}(\mathbf{r}_1,\mathbf{r}_2)+[S_F^{-1}*H_1*S_F^{-1}](\mathbf{r}_1,\mathbf{r}_2) . \tag{B2}$$

Consider now the eigenvalue problem

$$\int d^3r_2\{2\tilde{V}_{\text{p-h}}(\mathbf{r}_1,\mathbf{r}_2)+[S_F^{-1}*H_1*S_F^{-1}](\mathbf{r}_1,\mathbf{r}_2)\} \times H_1\psi^{(l)}(\mathbf{r}_2)=\hbar^2\omega_l^2\psi^{(l)}(\mathbf{r}_1) . \tag{B3}$$

The problem (B3) has the same structure as the eigenvalue problem discussed in papers I and II; in particular, the eigenvalues $\hbar^2\omega_l^2$ are real. It is then easily shown that the static form factor defined by Eq. (B2) has the form

$$S(\mathbf{r}_1,\mathbf{r}_2)=\sum_l \frac{1}{\hbar\omega_l}[H_1\psi^{(l)}(\mathbf{r}_1)][H_1\psi^{(l)}(\mathbf{r}_2)] , \tag{B4}$$

and the inverse, in the sense of the convolution product (2.5), is given by

$$S^{-1}(\mathbf{r}_1,\mathbf{r}_2)=\sum_l \hbar\omega_l\psi^{(l)}(\mathbf{r}_1)\psi^{(l)}(\mathbf{r}_2) . \tag{B5}$$

The set of non-nodal diagrams $X_{dd}(\mathbf{r}_1,\mathbf{r}_2)$ can now be obtained from Eq. (B1), and the function $\Gamma_{dd}(\mathbf{r}_1,\mathbf{r}_2)$ can be constructed from $S(\mathbf{r}_1,\mathbf{r}_2)$ through

$$\Gamma_{dd}(\mathbf{r}_1,\mathbf{r}_2)=[S_F^{-1}*S*S_F^{-1}](\mathbf{r}_1,\mathbf{r}_2)-S_F^{-1}(\mathbf{r}_1,\mathbf{r}_2) . \tag{B6}$$

We see that the solution of the Fermion PPA equation is hardly more involved than the solution of the corresponding Bose problem. The central step is the solution of the eigenvalue problem (B3) which is identical for Bose and Fermi statistics. The additional manipulations necessary in the Fermi case involve only the convolution products with S_F and S_F^{-1}.

APPENDIX C: SINGLE-PARTICLE DENSITIES AND THE TALMAN-SHADWICK EFFECTIVE POTENTIAL

We present in this appendix the detailed form of the one-body density and the density matrix generated by the single-particle wave functions (5.5) and the equations used to calculate the optimal one-body potential $U(z)$ [or equivalently, $V_F(z)$] of Eqs. (5.3) and (5.6). We assume periodicity in a box of length L parallel to the surface, and normalization of the z component of the wave function

$$\int_{-\infty}^{\infty} dz\,|\varphi_i(z)|^2=1 . \tag{C1}$$

The energy of a particle in state i with momentum $q_{||}$ parallel to the surface is

$$e_{i,q_{||}}=\epsilon_i+\frac{\hbar^2}{2m}q_{||}^2 . \tag{C2}$$

If the Fermi sea is filled up to a certain Fermi energy E_F, the total number of particles in a square piece of the film of sidelength L will be

$$N[E_F]=\sum_{e_{i\cdot q_{||}}\,(\le E_F)} 1 =L^2\sum_i \frac{\nu m}{2\pi\hbar^2}(E_F-\epsilon_i)\Theta(E_F-\epsilon_i) . \tag{C3}$$

[Actually, the argument is rigorous only if the single-particle orbitals are solutions of our full generalized Hartree-Fock equation (2.21). We assume here that the single-particle states generated by the approximation equations (5.2) and (5.5) are sufficiently close to the single-particle states generated by the full Hartree-Fock equation (2.21).] Equation (C3) is used to determine the Fermi energy from a given particle number N which is given by the requirement of charge neutrality, i.e.,

$$N=\rho_+L^2d . \tag{C4}$$

Given the Fermi energy, we can calculate the local-one-body density and the density matrix of the noninteracting system:

$$\rho_1^F(\mathbf{r},\mathbf{r}')=\rho_1^F(z,z',r_{||}) =\nu\int\frac{d^2q_{||}}{(2\pi)^2}\sum_i\Theta\left[E_F-\epsilon_i-\frac{\hbar^2}{2m}q_{||}^2\right]\varphi_i^*(z) \times\varphi_i(z')\exp[i\mathbf{q}_{||}\cdot(\mathbf{r}_{||}-\mathbf{r}'_{||})] \tag{C5}$$

and

$$\rho_1(z)=\frac{\nu m}{2\pi\hbar^2}\sum_i\Theta(E_F-\epsilon_i)(E_F-\epsilon_i)\,|\varphi_i(z)|^2 . \tag{C6}$$

The static form factor of the uncorrelated system, S_F, is needed in a representation, where the coordinate parallel to the surface is Fourier transformed,

$$S_F(z,z',q_{||})=\delta(z-z')-\frac{1}{\nu}\frac{\int d^2r_{||}\,|\rho_1^F(z,z',r_{||})|^2e^{ir_{||}\cdot q_{||}}}{[\rho_1(z)\rho_1(z')]^{1/2}} . \tag{C7}$$

Inserting the representation (C5) leads us to

$$S_F(z,z',q_{||})=\delta(z-z') -\frac{\sum_{i,j}N(i,j,q_{||})\varphi_i(z)\varphi_i^*(z')\varphi_j^*(z)\varphi_j(z')}{[\rho_1(z)\rho_1(z')]^{1/2}} , \tag{C8}$$

where

$$N(i,j,q_{||})=\nu\int\frac{d^2q}{(2\pi)^2}\Theta\left[E_F-\epsilon_i-\frac{\hbar^2}{2m}q^2\right] \times\Theta\left[E_F-\epsilon_j-\frac{\hbar^2}{2m}(\mathbf{q}_{||}-\mathbf{q})^2\right] . \tag{C9}$$

We now calculate the variation of the total ground-state energy with respect to the effective one-body potential $U(z)$. The energy depends on $U(z)$ only through the

single-particle orbitals $\varphi(z)$, i.e.,

$$\frac{\delta E}{\delta U(z)}=\sum_i \int dz' \frac{\delta E}{\delta \varphi_i^*(z')}\frac{\delta \varphi_i^*(z')}{\delta U(z)}+\text{c.c.}=0 . \tag{C10}$$

The single-particle states $\varphi_i(z)$ are determined through (5.3) by the effective one-body potential $U(z)$. Using first-order perturbation theory, Talman and Shadwick[17] found that

$$\frac{\delta \varphi_i^*(z')}{\delta U(z)}=-\sum_{j\,(\neq i)} \frac{\varphi_j^*(z')\varphi_j(z)}{\epsilon_j-\epsilon_i}\varphi_i^*(z) . \tag{C11}$$

For the case of our geometry, the summation over the occupied states appearing in Eq. (C10) involves integration over the momentum $\mathbf{q}_{||}$ parallel to the surface. Carrying out these phase-space integrations and using the fact that $\delta\varphi_i^*(z')/\delta U(z)$ projects into a subspace orthogonal to $\varphi_i^*(z)$, we finally find the condition

$$0=\sum_i \int \frac{d^2q}{(2\pi)^2}\Theta\left[E_F-\epsilon_i-\frac{\hbar^2}{2m}q^2\right]\int dz_1 \frac{\delta\varphi_i^*(z_1)}{\delta U(z)}[V_H(z_1)-U(z_1)]\varphi_i(z_1)$$
$$-\sum_{i,j}\int \frac{d^2q_{||}}{(2\pi)^2}\int dz_1\int dz_2\, N(i,j;q_{||})V_F(z_1,z_2,q_{||})\varphi_j(z_1)\varphi_j^*(z_2)\varphi_i(z_2)\frac{\delta\varphi_i^*(z_1)}{\delta U(z)}+\text{c.c.} , \tag{C12}$$

where

$$V_F(z_1,z_2,q_{||})=\int d^2r_{||}\, V_F(z_1,r_2,r_{||})e^{i\mathbf{r}_{||}\cdot\mathbf{q}_{||}} . \tag{C13}$$

Inserting (C10) and $V_{\rm TS}(z)\equiv V_H(z)-U(z)$, we finally arrive at the compact form of the optimization condition for the effective one-body potential

$$\sum_{j\,(\neq i)}\Theta(E_F-\epsilon_j)\frac{\varphi_i(z)\varphi_j^*(z)}{\epsilon_j-\epsilon_i}\left[\frac{\nu m}{2\pi\hbar^2}(E_F-\epsilon_j)U_{ij}-V_{ij}\right]=0 \tag{C14}$$

with

$$U_{ij}=\int dz\,\varphi_i(z)\varphi_j^*(z)V_{\rm TS}(z) \tag{C15}$$

and

$$V_{ij}\equiv-\int\frac{d^2q_{||}}{(2\pi)^2}\int dz_1\int dz_2\sum_k N(k,j;q_{||})V_F(z_1,z_2,q_{||})\varphi_i^*(z_1)\varphi_k(z_1)\varphi_k^*(z_2)\varphi_j(z_2) . \tag{C16}$$

With the definitions (C15) and (C16), Eq. (C14) is a linear equation for the unknown function $V_{\rm TS}(z)$ which can be solved for any given Fock term $V_F(\mathbf{r}_1,\mathbf{r}_2)$. Note that, due to the orthogonality of the single-particle states $\varphi_i(z)$, the effective interaction is determined only up to an additive constant.

*On leave. Present address: Max-Planck-Institut für Kernphysik, D-6900 Heidelberg, West Germany.

†Present address: Xerox Corporation, Palo Alto Research Center, 3333 Coyote Hill Road, Palo Alto, CA 94304.

[1]W. Kohn and P. Vashista, in *Theory of the Inhomogeneous Electron Gas*, edited by S. Lundqvist and N. H. March (Plenum, New York, 1983), pp. 79ff.

[2]D. C. Langreth and M. J. Mehl, Phys. Rev. B **28**, 1809 (1983).

[3]D. M. Ceperley and B. J. Alder, Phys. Rev. Lett. **45**, 566 (1980).

[4]E. Krotscheck, G.-X. Qian, and W. Kohn, Phys. Rev. B **31**, 4245 (1985) (paper I).

[5]E. Krotscheck, Phys. Rev. B **31**, 4258 (1985) (paper II).

[6]E. Krotscheck, Phys. Rev. B **31**, 4267 (1985) (paper III).

[7]F. D. Mackie and C.-W. Woo, Phys. Rev. B **17**, 2877 (1978); C.-W. Woo, in *Proceedings of the Third International Conference on Recent Progress in Many-Body Theories*, edited by H. Kümmel and M. L. Ristig (Springer, Berlin, 1984); X. Sun, T. Li, and C.-W. Woo, Acta Phys. Sin. (China) **31**, 1466 (1982); **31**, 1474 (1982).

[8]X. Sun, T. Li, M. Farjam, and C.-W. Woo, Phys. Rev. B **27**, 3913 (1983); X. Sun, M. Farjam, and C.-W. Woo, *ibid* **28**, 5599 (1983).

[9]E. Krotscheck and M. L. Ristig, Nucl. Phys. **242A**, 389 (1975); E. Krotscheck, J. Low Temp. Phys. **27**, 199 (1977).

[10]E. Feenberg, *Theory of Quantum Fluids* (Academic, New York, 1969).

[11]M. Gaudin, J. Gillespie, and G. Ripka, Nucl. Phys. **176A**, 237 (1971).

[12]J. W. Clark, in *Progress in Particle and Nuclear Physics*, edited by D. H. Wilkinson (Pergamon, Oxford, 1979), Vol. 2, p. 89.

[13]C. E. Campbell and E. Feenberg, Phys. Rev. **188**, 396 (1969).

[14]E. Krotscheck, Ann. Phys. (N.Y.) **155**, 1 (1984).

[15]E. Krotscheck and J. W. Clark, Nucl. Phys. **328A**, 73 (1979).

[16]E. Krotscheck, R. A. Smith, J. W. Clark, and R. M. Panoff, Phys. Rev. B **24**, 6383 (1981).

[17]J. D. Talman and W. F. Shadwick, Phys. Rev. A **14**, 36 (1976).

[18]V. Sahni and C. Q. Ma, Phys. Rev. B **22**, 5987 (1982).

[19]K. T. R. Davies, H. Flocard, S. Krieger, and M. S. Weiss,

Nucl. Phys. **342A**, 111 (1980).
[20]N. D. Lang and W. Kohn, Phys. Rev. B **1**, 4555 (1970).
[21]N. W. Ashcroft, Phys. Lett. **23**, 48 (1966).
[22]R. Monnier and J. P. Perdew, Phys. Rev. B **17**, 2595 (1978).
[23]V. Sahni and J. Gruenebaum, Phys. Rev. B **19**, 1840 (1979); V. Sahni, J. P. Perdew, and J. Gruenebaum, Phys. Rev. B **23**, 6512 (1981).
[24]W. R. Tyson and W. A. Miller, Surf. Sci. **62**, 267 (1977).
[25]H. Warwa, Z. Metallk. **66**, 395, 492 (1975).
[26]E. S. Levin, G. D. Ayushina, and P. V. Gel'd, High Temp. (USSR) **6**, 416 (1968).
[27]D. W. G. White, Trans. Metall. Soc. AIME **236**, 796 (1966).
[28]J. Bohdansky and H. E. J. Schins, J. Inorg. Nucl. Chem. **29**, 2173 (1967); **30**, 2331 (1968).
[29]D. Germer and H. Mayer, Z. Phys. **210**, 391 (1968).
[30]N. D. Lang and W. Kohn, Phys. Rev. B **3**, 1215 (1971).
[31]D. Ceperley, Phys. Rev. B **18**, 3126 (1978).
[32]R. A. Smith and A. D. Jackson (unpublished); R. A. Smith (private communication).